Non-deletional CD8+ T cell self-tolerance permits responsiveness but limits tissue damage

Emily Nestor Truckenbrod[1], Kristina S Burrack[1,2], Todd P Knutson[3], Henrique Borges da Silva[1,4], Katharine E Block[1], Katie R Stagliano[5], Arthur A Hurwitz[6], Ross B Fulton[1,7], Kristin R Renkema[1,8*], Stephen C Jameson[1*]

[1]Center for Immunology, University of Minnesota; [2]Current address: Hennepin Healthcare Research Institute; [3]Minnesota Supercomputing Institute, University of Minnesota; [4]Current address: Mayo Clinic Arizona; [5]NIAID, NIH; [6]AgenTus Therapeutics, Inc.; [7]Current address: iFiBiO Therapeutics, [8]Current address: Grand Valley State University

[*]Corresponding authors

Stephen Jameson: james024@umn.edu, ORCID: 0000-0001-9137-1146
Kristin Renkema: renkemak@gvsu.edu , ORCID: 0000-0003-4000-3356

Abstract

Self-specific CD8+ T cells often escape clonal deletion, but the properties and capabilities of such cells in a physiological setting are unclear. We characterized polyclonal $CD8^+$ T cells specific for the melanocyte antigen tyrosinase-related protein 2 (Trp2) in mice that express or lack this enzyme due to deficiency in *Dct*, which encodes Trp2. The size, phenotype, and gene expression profile of the pre-immune Trp2/K^b-specific pool were similar in wild-type (WT) and *Dct*-deficient (*Dct*$^{-/-}$) mice. Despite comparable initial responses to Trp2 immunization, WT Trp2/K^b-specific cells showed blunted expansion, and scRNAseq revealed WT cells less readily differentiated into a CD25+ proliferative population. Functional self-tolerance clearly emerged when assessing immunopathology: adoptively transferred WT Trp2/K^b-specific cells mediated vitiligo much less efficiently. Hence, $CD8^+$ T cell self-specificity is poorly predicted by precursor frequency, phenotype or even initial responsiveness, while deficient activation-induced CD25 expression and other gene expression characteristics may help to identify functionally tolerant cells.

Introduction

Accurate discrimination between harmful (pathogens, toxins, cancerous cells) and non-harmful entities (self, innocuous environmental components, non-pathogenic microbes) underlies effective functioning of the immune system. Understanding the mechanisms that normally enforce immunological tolerance to self is a prerequisite for safely and effectively manipulating the immune system to therapeutically induce or break self-tolerance.

Tolerance can be mediated by the clonal deletion of developing self-reactive T cells (Hogquist et al., 2005; Kappler et al., 1987). Largely based on studies in transgenic mouse models, this process has long been regarded as common and highly efficient (Palmer, 2003). However, recent studies have revealed that thymic clonal deletion is less effective than previously thought (Richards et al., 2016). Self-reactive CD8+ T cells have been shown to escape negative selection in mice (Bouneaud et al., 2000; Zehn & Bevan, 2006), with one group proposing that up to 4% of peripheral CD8+ T cells are self-specific (Richards et al., 2015). Furthermore, studies in humans indicated that precursor frequencies of blood CD8+ T cells specific for certain self-peptides were comparable to those demonstrated for foreign peptides (Yu et al., 2015) and suggested that such cells might be capable of overt autoreactivity if suitably stimulated (Maeda et al., 2014).

Aside from clonal deletion, tolerance mechanisms include ignorance of antigen, suppression by regulatory T cells (Tregs), and induction of a functionally unresponsive or hyporesponsive anergic state (Mescher et al., 2007; Mueller, 2010; Redmond & Sherman, 2005; Schietinger & Greenberg, 2014). However, different models have produced conflicting evidence regarding the contribution of each of these mechanisms and whether non-deletional $CD8^+$ T cell tolerance is an intrinsic property of tolerant cells (Yu et al., 2015) or dependent on restraint by Tregs (Maeda et al., 2014; Richards et al., 2015). It is also unclear how the presence and reactivity of self-specific $CD8^+$ T cells relates to their ability to drive immunopathology. The majority of commonly-used mouse models of tolerance have the drawbacks of relying on T cell receptor (TCR) transgenic animals that may not recapitulate normal physiology or utilizing in vitro analyses for characterization of functionality.

Our studies are intended to provide a better understanding of non-deletional CD8+ T cell tolerance by utilizing a more physiologic and translationally-relevant mouse model in which an epitope from the melanocyte differentiation enzyme tyrosinase-related protein 2 (Trp2) is recognized by CD8+ T cells as either self or foreign. Tyrosinase-related protein 2, an enzyme involved in melanin biosynthesis encoded by the dopachrome tautomerase (*Dct*) gene, is normally expressed by melanocytes in the skin in both humans and C57BL/6 mice and is overexpressed by many melanomas (Avogadri et al., 2016; Wang et al., 1996). Using wild-type (WT) mice and a novel *Dct*-deficient ($Dct^{-/-}$) strain, we compared responses to $Trp2_{180\text{-}188}/K^b$ (Trp2/K^b) as a self- versus foreign antigen. This model is relevant to human health, as Trp2 is a common

target in cancer immunotherapy directed against melanoma (Cho & Celis, 2009; Liu et al., 2014; Parkhurst et al., 1998), and Trp2/K^b-specific responses can be induced in WT mice with vigorous priming approaches (Bowne et al., 1999; Byrne et al., 2011; Cho & Celis, 2009). Instead of utilizing TCR transgenic models, we focus on the polyclonal Trp2/K^b-specific CD8+ T cell repertoire to maximize applicability to normal physiology.

Here, we show that tolerance among Trp2/K^b-specific $CD8^+$ T cells is manifest primarily at the level of minimizing overt autoimmunity, with few differences in the size, phenotype, and initial Trp2 responsiveness of the precursor pool in WT and *Dct*$^{-/-}$ mice. The underlying tolerance mechanism does not depend on cell-extrinsic regulation but rather correlates with a cell-intrinsic failure of WT Trp2/K^b-specific $CD8^+$ T cells to sustain optimal proliferation. However, while differences in the responsiveness of WT and *Dct*$^{-/-}$ cells to Trp2 immunization were mostly subtle, a notable difference emerged when the cells were assessed for their ability to provoke autoimmune vitiligo: cells primed in *Dct*$^{-/-}$ mice were much more effective than those primed in WT animals. Accordingly, we conclude that tolerance does not markedly impact the presence, phenotype, or initial reactivity of Trp2/K^b-specific $CD8^+$ T cells but severely limits whether these cells are capable of overt autoreactivity. Moreover, our polyclonal model reveals that certain characteristics of Trp2/K^b-responsive effector cells— reduced CD25 expression and impaired differentiation into a highly proliferative subpopulation — correlate with functional tolerance of a T cell population, providing a framework for future characterization of self-specific $CD8^+$ T cells.

Results

The pre-immune population of Trp2/K^b-specific cells is similarly sized and appears naïve in WT and Dct$^{-/-}$ mice

Clonal deletion is a well-studied tolerance mechanism that may result in the near-total culling of self-specific cells or at least a marked reduction and reduced apparent TCR affinity of surviving self-specific cells (Bouneaud et al., 2000; Cheng & Anderson, 2018; Enouz et al., 2012; Hogquist et al., 2005; Zehn & Bevan, 2006). We assessed the number and phenotype of Trp2/K^b-specific cells in pre-immune (naïve) mice to examine deletional central tolerance in our model. For mice in which Trp2 would not be a self-antigen, we used a novel *Dct*$^{-/-}$ strain that carries a large deletion encompassing the exon encoding Trp2$_{180\text{-}188}$, unlike a previously described *Dct*-targeted strain that retains the coding sequence for that epitope (Guyonneau et al., 2004). We performed tetramer enrichment from the spleen and lymph nodes of pre-immune WT and *Dct*$^{-/-}$ mice to quantify the number of Trp2/K^b-specific CD8+ T cell precursors (Figure 1A, S1A). While we identified slightly more antigen-specific cells in *Dct*$^{-/-}$ mice, we nevertheless found relatively large numbers of Trp2/K^b-specific CD8+ T cells (> 1500) in both strains, evidence that most Trp2/K^b-specific cells escape thymic or peripheral clonal deletion in WT mice.

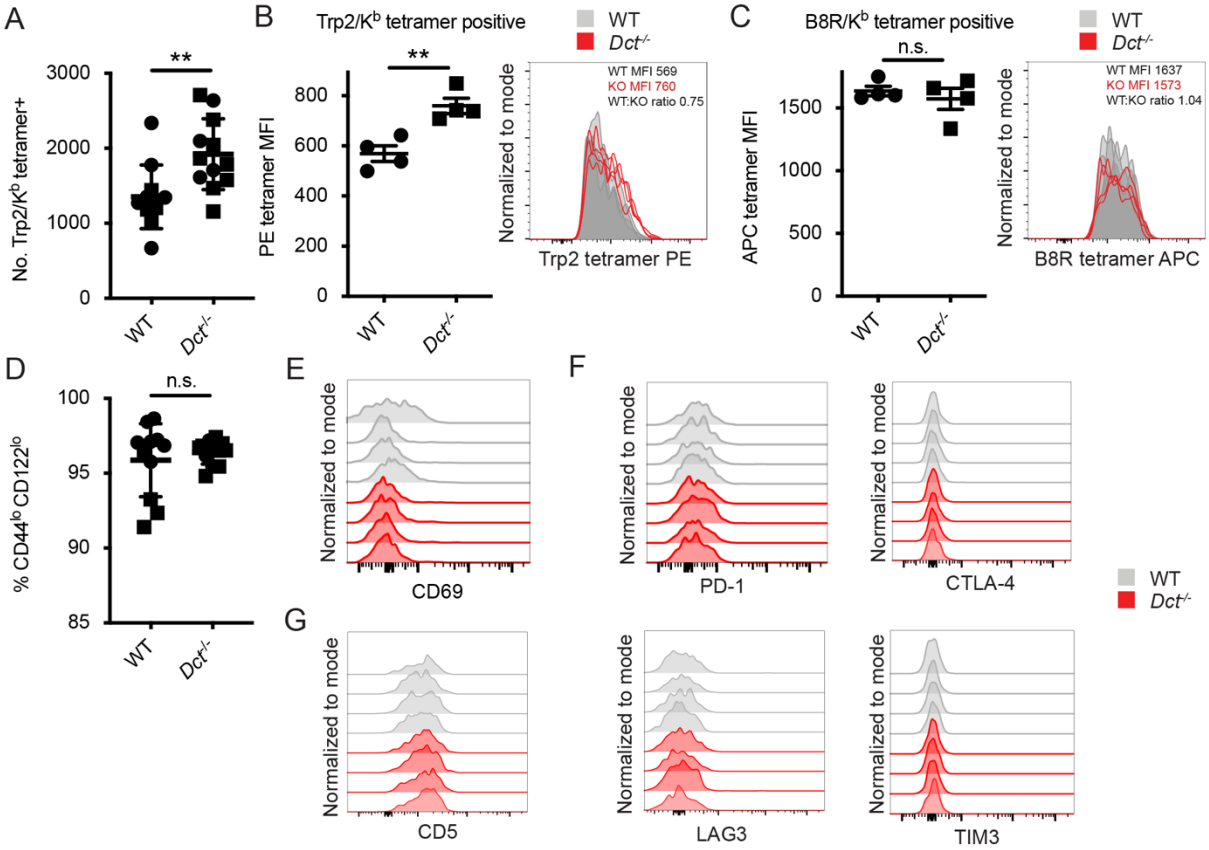

Figure 1. Trp2/K^b-specific CD8+ T cells in pre-immune WT and *Dct*$^{-/-}$ mice share a naïve phenotype while showing modest differences in frequency and tetramer staining
Tetramer enrichment was performed to enumerate Trp2/K^b-specific CD8+ T cells per mouse (A). Median tetramer fluorescence intensity (MFI) was used to estimate the avidity of enriched Trp2/K^b-specific (B) or B8R/K^b-specific cells (C). (D) CD44/CD122 expression of Trp2/K^b-specific cells. (E) CD69 expression of Trp2/K^b-specific cells . (F) PD-1, CTLA-4, LAG3, and TIM3 expression of Trp2/K^b-specific cells. (G) CD5 expression of Trp2/K^b-specific cells. Data are compiled from three independent experiments in A and D. Four WT and *Dct*$^{-/-}$ mice are shown in B and C; results are representative of other experiments. The graphs in Figures 1E–G represent individual experiments with four mice per group. Squares indicate male animals. ** $p < 0.01$ by unpaired t test.

In some systems, T cells bearing TCRs with low affinity for self-antigens avoid deletion; low affinity TCRs can often be identified by reduced peptide/MHC tetramer binding to these cells (Bouneaud et al., 2000; Daniels & Jameson, 2000; Daniels et al., 2006; Enouz et al., 2012; Hogquist et al., 2005; Zehn & Bevan, 2006; Zehn et al., 2009). We compared the Trp2/K^b tetramer median fluorescence intensity (MFI) in pre-immune WT and *Dct*$^{-/-}$ mice. The average Trp2/K^b tetramer staining was higher on *Dct*$^{-/-}$ cells, but the MFI largely overlapped between the two populations (Figure 1B), suggesting that the range of TCR avidities did not markedly differ between the Trp2/K^b-specific pools. Indeed, the tetramer staining differences we observed (a WT:*Dct*$^{-/-}$ tetramer MFI ratio of ~0.75) are more subtle than that noted in a previous study using a transgenic mouse model, which reported a tetramer ratio of ~0.35 between mice with vs. without self-antigen expression (Bouneaud et al., 2000). As a control, we also assessed the avidity of cells specific for an irrelevant foreign epitope—B8R/K^b from vaccinia virus—in WT and *Dct*$^{-/-}$ mice; the tetramer MFI of B8R/K^b-specific cells was comparable between the strains (Figure 1C).

We also examined the phenotype of Trp2/K^b-specific cells in pre-immune WT and *Dct*$^{-/-}$ mice. No consistent differences in the expression of activation/memory markers (CD69, CD44, CD122) or anergy/exhaustion markers (PD-1, LAG3, CTLA-4, TIM3) were identified between *Dct*$^{-/-}$ and WT Trp2/K^b-specific cells (Figures 1C–F, S1B, S1C). The majority of cells exhibited low expression of the memory markers CD44 and CD122, and anergy/exhaustion marker expression was low in both populations. CD5 can indicate self-antigen recognition (Azzam et al., 1998; Fulton et al., 2015), but we did not detect significant differences in expression between the groups (Figure 1G). RNAseq analysis of Trp2/K^b tetramer-binding cells isolated from pre-immune mice by fluorescence-activated cell sorting (FACS) showed no consistent differences in gene expression related to their derivation from WT versus *Dct*$^{-/-}$ mice (Supplemental figure 1D), although this does not rule out the possibility of epigenetic differences between the populations.

To ensure our findings were not unique to Trp2$_{180}$/K^b-specific cells, we used tetramer enrichment to isolate CD8+ T cells specific for other skin antigens—a distinct Trp2 epitope (Trp2$_{363}$/D^b) and a tyrosinase-related protein 1 epitope (Trp1$_{455}$/D^b)—in mice expressing or lacking these antigens. We were able to identify cells with these specificities present at numbers similar to slightly less in mice expressing antigen

relative to mutant mice (Supplemental figure 1E). This suggests that CD8+ T cells specific for other melanocyte self-epitopes also largely escape clonal deletion.

Hence, although we identified some minor differences between Trp2/K^b-specific cells from WT versus *Dct*$^{-/-}$ mice, these pre-immune populations generally resembled each other in number, phenotype, and gene expression, arguing against a major role for clonal deletion or overt steady-state anergy induction as tolerance mechanisms to this antigen. These findings resonate with studies in humans, which have shown that the precursor frequency and peptide/MHC tetramer staining intensity were only modestly reduced for a self- versus non-self antigen (Yu et al., 2015) and that self-specific cells can be phenotypically naïve (Maeda et al., 2014; Yu et al., 2015). Accordingly, these data suggested that analysis of the Trp2/K^b-specific responses in mice could serve as a useful model to investigate the basis for and limits of non-deletional self-tolerance.

WT Trp2/K^b-specific CD8+ T cells display impaired responses to Trp2 immunization

It was possible that the lack of substantial clonal deletion or signs of prior activation in WT Trp2/K^b-specific cells indicated "ignorance" of Trp2 and/or that the $Trp2_{180}$ epitope, which shows suboptimal binding to K^b (McWilliams et al., 2006), was unable to prime a vigorous immune response. To investigate this, we challenged WT and *Dct*$^{-/-}$ mice with Trp2 in an immunogenic context using TriVax, a subunit immunization strategy comprising peptide, agonist anti-CD40 antibody, and poly(I:C) (Cho & Celis, 2009). It should be noted that the TriVax approach uses the minimal peptide for priming, which likely excludes antigen-specific Treg involvement. We included B8R peptide in addition to Trp2 peptide in these experiments as an internal control. While WT and *Dct*$^{-/-}$ mice responded similarly to B8R, WT mice showed a more limited response to Trp2 at an effector time point (day 7) relative to *Dct*$^{-/-}$ mice (Figure 2A, B), ruling out ignorance as the dominant tolerance mechanism. We observed a significantly larger number and frequency of Trp2/K^b-specific cells in *Dct*$^{-/-}$ mice, and the *Dct*$^{-/-}$ cells exhibited higher apparent Trp2/K^b avidity (as measured by tetramer MFI; Figure 2C–E). Still, WT Trp2/K^b-specific cells expanded > 1000-fold (*Dct*$^{-/-}$ cells expanded ~4000-fold). The WT:*Dct*$^{-/-}$ tetramer ratio was little changed relative to the pre-immune populations, suggesting the difference in avidity between WT and *Dct*$^{-/-}$ cells had not been amplified by activation. The frequency of PD-1+ cells was comparable between WT and *Dct*$^{-/-}$ Trp2/K^b-specific populations at this time point (Figure 2F), suggesting similar exposure to antigen.

To ensure that our results were not specific to the TriVax system, we also infected mice with a recombinant *Listeria monocytogenes* strain expressing Trp2 (LmTrp2) (Bruhn et al., 2005) and sacrificed the mice at effector (day 7) and memory (day 45) time points, assessing the percentage and number of Trp2/K^b-specific CD8+ T cells and cytokine production in response to ex vivo Trp2 stimulation. Again, the Trp2/K^b-specific response was greater in *Dct*$^{-/-}$ mice at both effector and memory time points (Supplemental figures 2A–C). Similarly, the frequency of all CD8+ T cells responding to ex vivo Trp2 stimulation with cytokine production (IFN-γ, TNF-α) was larger in *Dct*$^{-/-}$ mice; the percent producing IFN-γ approximated the tetramer-positive population, suggesting that the

majority of Trp2/K^b-specific cells were able to produce this cytokine in both strains of mice (Supplemental figure 2D). Among IFN-γ-producing cells, those from *Dct*$^{-/-}$ mice tended to produce increased amounts of cytokine on a per-cell basis (as assessed by IFN-γ MFI).

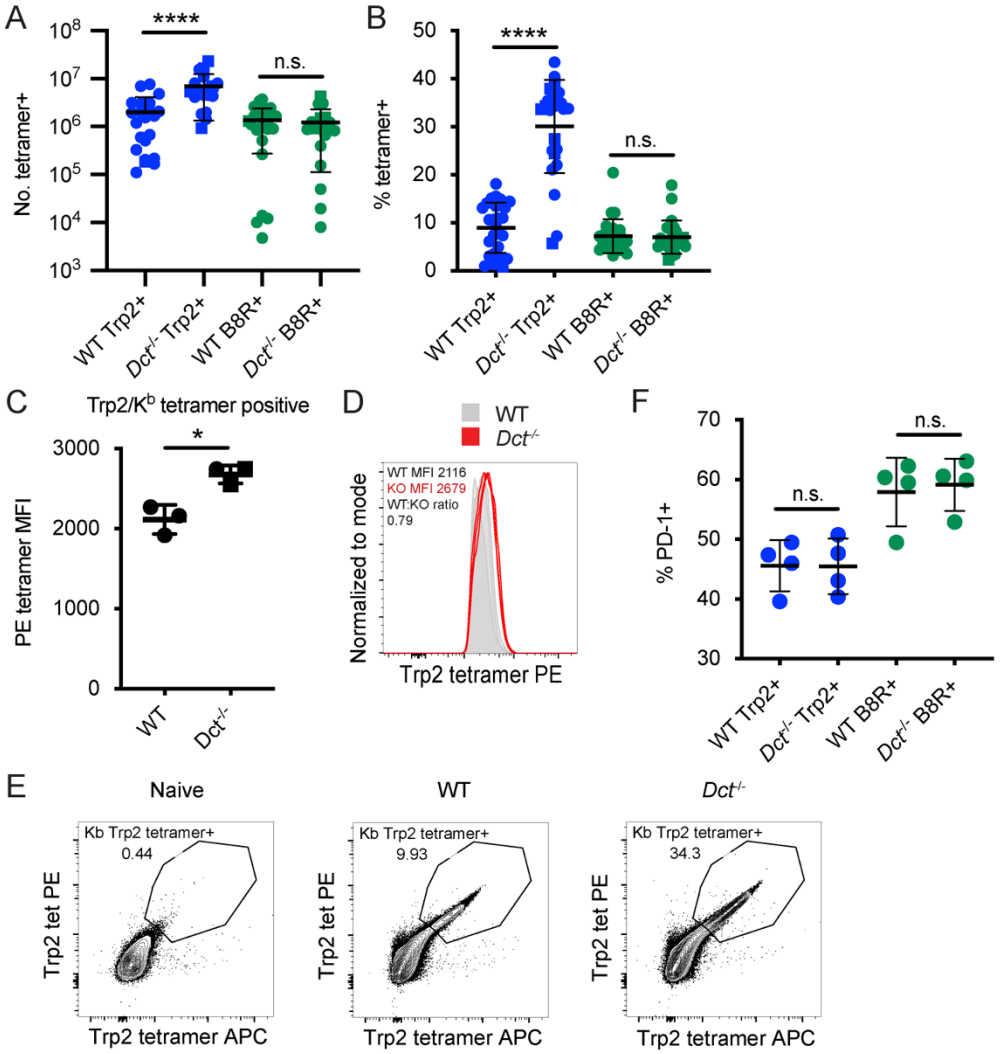

Figure 2. WT and *Dct*$^{-/-}$ Trp2/K^b-specific cells respond differently to immunization with Trp2
Mice were primed with TriVax (50 ug each of Trp2 and B8R peptides; A–F). The number (A) or percent (B) of splenic Trp2/K^b or B8R/K^b-specific cells was assessed at the day seven. (C, D) The tetramer fluorescence intensity of splenic Trp2/K^b-specific cells was compared. (E) Gating for dual Trp2/K^b tetramer positive CD8+. (F) The frequency of the indicated splenic population expressing PD-1 is shown. Data in A and B are compiled from more than three experiments. Data in C–F are representative of three or more similar experiments. Squares indicate male animals. * $p < 0.05$, **** $p < 0.0001$ by unpaired t test (C) or one-way ANOVA with Sidak's multiple comparisons test (A, B, F).

Tolerance to Trp2/K^b is CD8$^+$ T cell-intrinsic

Both cell-intrinsic and cell-extrinsic mechanisms of CD8+ T cell tolerance have been previously described. Sakaguchi's group (Maeda et al., 2014) identified anergic CD8+ T cells specific for melanocyte antigens in healthy human donors and concluded that

these cells were restrained by Tregs. In contrast, other groups have shown cell-intrinsic deficits among self-reactive CD8+ T cells. For example, Davis' group (Yu et al., 2015) found human self-antigen-specific T cells to be poorly responsive to antigenic stimulation even in the absence of Tregs, and Greenberg and colleagues (Schietinger et al., 2012) showed that tolerant self-reactive murine CD8+ T cells remained tolerant when transferred into new hosts that lacked antigen expression.

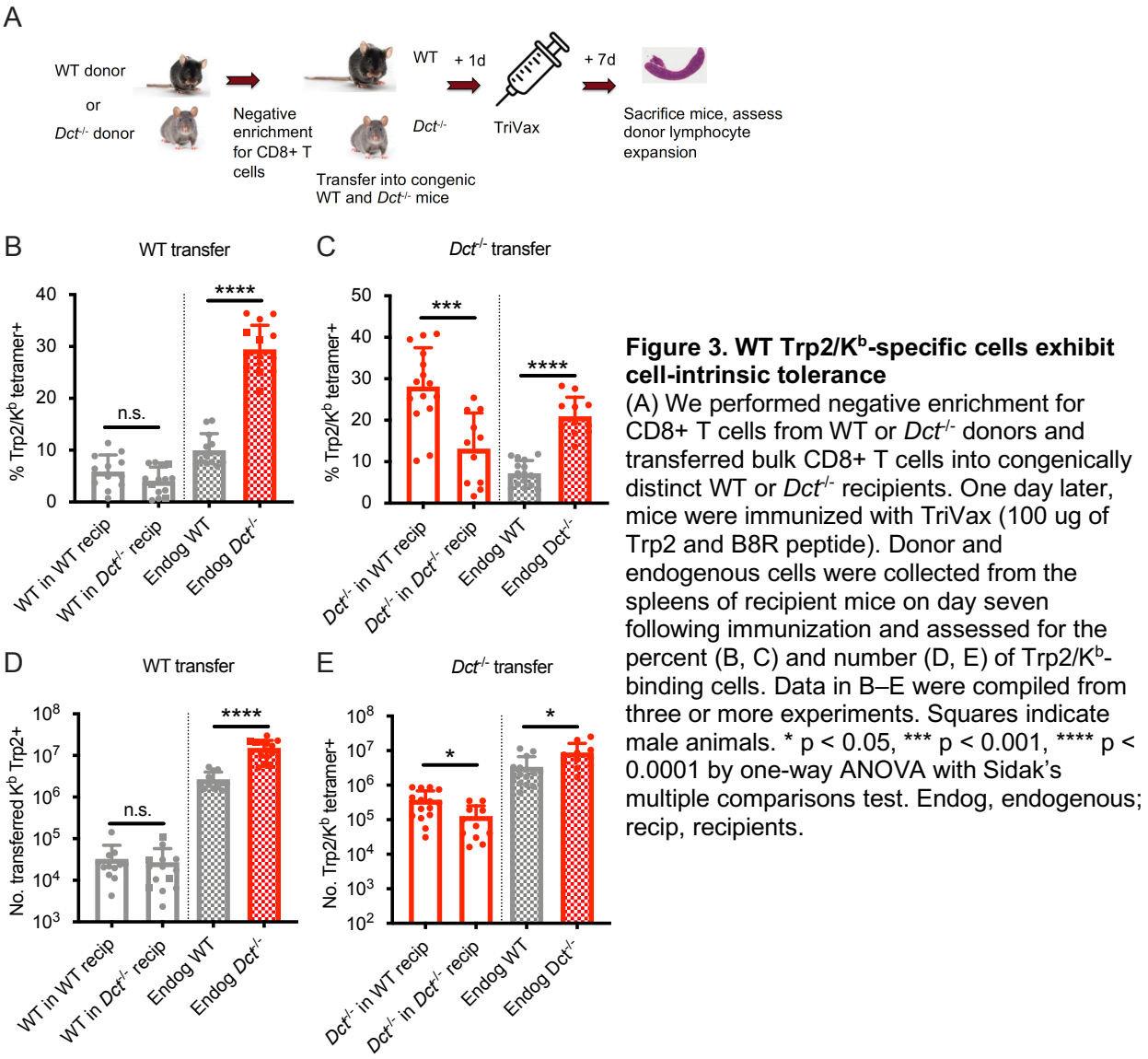

Figure 3. WT Trp2/K^b-specific cells exhibit cell-intrinsic tolerance
(A) We performed negative enrichment for CD8+ T cells from WT or *Dct*$^{-/-}$ donors and transferred bulk CD8+ T cells into congenically distinct WT or *Dct*$^{-/-}$ recipients. One day later, mice were immunized with TriVax (100 ug of Trp2 and B8R peptide). Donor and endogenous cells were collected from the spleens of recipient mice on day seven following immunization and assessed for the percent (B, C) and number (D, E) of Trp2/K^b-binding cells. Data in B–E were compiled from three or more experiments. Squares indicate male animals. * $p < 0.05$, *** $p < 0.001$, **** $p < 0.0001$ by one-way ANOVA with Sidak's multiple comparisons test. Endog, endogenous; recip, recipients.

Accordingly, we investigated whether cell-intrinsic or -extrinsic mechanisms were active in restraining Trp2/K^b-specific CD8+ T cells in WT mice. To assess this, we transferred bulk WT polyclonal CD8+ T cells to both WT and *Dct*$^{-/-}$ recipients, then primed the mice with TriVax and examined the effector response at day 7 post-immunization (Figure 3A, 3B, 3D). Transferred WT Trp2/K^b-specific cells did proliferate (~100-fold expansion), albeit to a much lesser degree than endogenous *Dct*$^{-/-}$ Trp2/K^b-specific cells. Importantly, their expansion was comparable in both WT and *Dct*$^{-/-}$ recipients (Figure

3B, D), suggesting that the WT CD8$^+$ T cells remained hyporesponsive even in an environment where endogenous cells were not tolerant to Trp2, supporting a cell-intrinsic basis for the impaired reactivity of WT Trp2/K^b-specific CD8$^+$ T cells.

We also assessed the performance of *Dct*$^{-/-}$ CD8$^+$ T cells when transferred into *Dct*$^{-/-}$ and WT hosts prior to priming to determine whether they would acquire tolerance in the WT environment (Figure 3A). These Trp2/K^b-specific donor cells were able to expand robustly in both *Dct*$^{-/-}$ and WT recipients (Figure 3C, E), further demonstrating a lack of extrinsic regulation in the WT environment. *Dct*$^{-/-}$ cells actually performed better in WT recipients than in *Dct*$^{-/-}$ recipients; the basis for this outcome is not clear but could be due to reduced competition by endogenous Trp2/K^b-specific cells in WT hosts. Preliminary studies indicated that *Dct*$^{-/-}$ cells still showed strong expansion when the interval between cell transfer and TriVax was extended from one day to one week, suggesting that these cells did not acquire tolerance characteristics within this timeframe (data not shown).

We conducted similar transfers utilizing LmTrp2 instead of TriVax, again finding evidence of cell-intrinsic tolerance. The transferred cells behaved in accordance with the donors' Trp2 expression rather than that of the recipients: WT cells remained tolerant when primed in *Dct*$^{-/-}$ recipients, while *Dct*$^{-/-}$ cells retained the ability to expand when primed in WT recipients (Supplemental figure 2E, 2F). Collectively, these data indicate that cell-intrinsic mechanism(s) enforce tolerance among WT Trp2/K^b-specific cells.

WT Trp2/K^b-specific cells are capable of an acute response to Trp2

Although the response to Trp2 immunization was weaker in WT versus *Dct*$^{-/-}$ mice, the WT response was still substantial (Figure 2A). Studies on T cells with low affinity TCRs have shown a normal initial proliferative response that stalls prematurely relative to the response by high affinity T cells (Enouz et al., 2012; Ozga et al., 2016; Zehn et al., 2009). Alternatively, it was possible that fewer clones would be recruited into the Trp2 response in WT mice, leading to decreased expansion relative to *Dct*$^{-/-}$ animals from the initiation of an immune response. To distinguish between these possibilities, we studied the expansion kinetics of the Trp2/K^b-specific response in WT and *Dct*$^{-/-}$ mice. In order to track early polyclonal responses, TriVax with a higher dose of Trp2 peptide was used in these studies, and tetramer enrichment was used to isolate Trp2/K^b-specific cells. Interestingly, WT Trp2/K^b-specific cells were capable of an initial response that largely paralleled that shown by their *Dct*$^{-/-}$ counterparts (Figure 4A). One day after TriVax immunization, few cells were isolated, likely due to either trapping within the tissues (Weninger et al., 2001) or TCR downregulation (Cai et al., 1997). Slightly more Trp2/K^b-specific cells were identified in WT mice on day two, while increased numbers of Trp2/K^b-specific cells were seen in *Dct*$^{-/-}$ mice on days three through five. By days six and seven after high dose TriVax immunization, Trp2/K^b-specific cells in *Dct*$^{-/-}$ mice outnumbered those in WT mice by an average ratio of 4:1. Although significant, these differences in expansion were modest in comparison with the > 1000-fold expansion of Trp2/K^b-specific cells in both strains (Figure 4A). Preliminary assessment of apoptosis

induction (annexin V staining) showed no differences between the strains at one or three days after TriVax (data not shown).

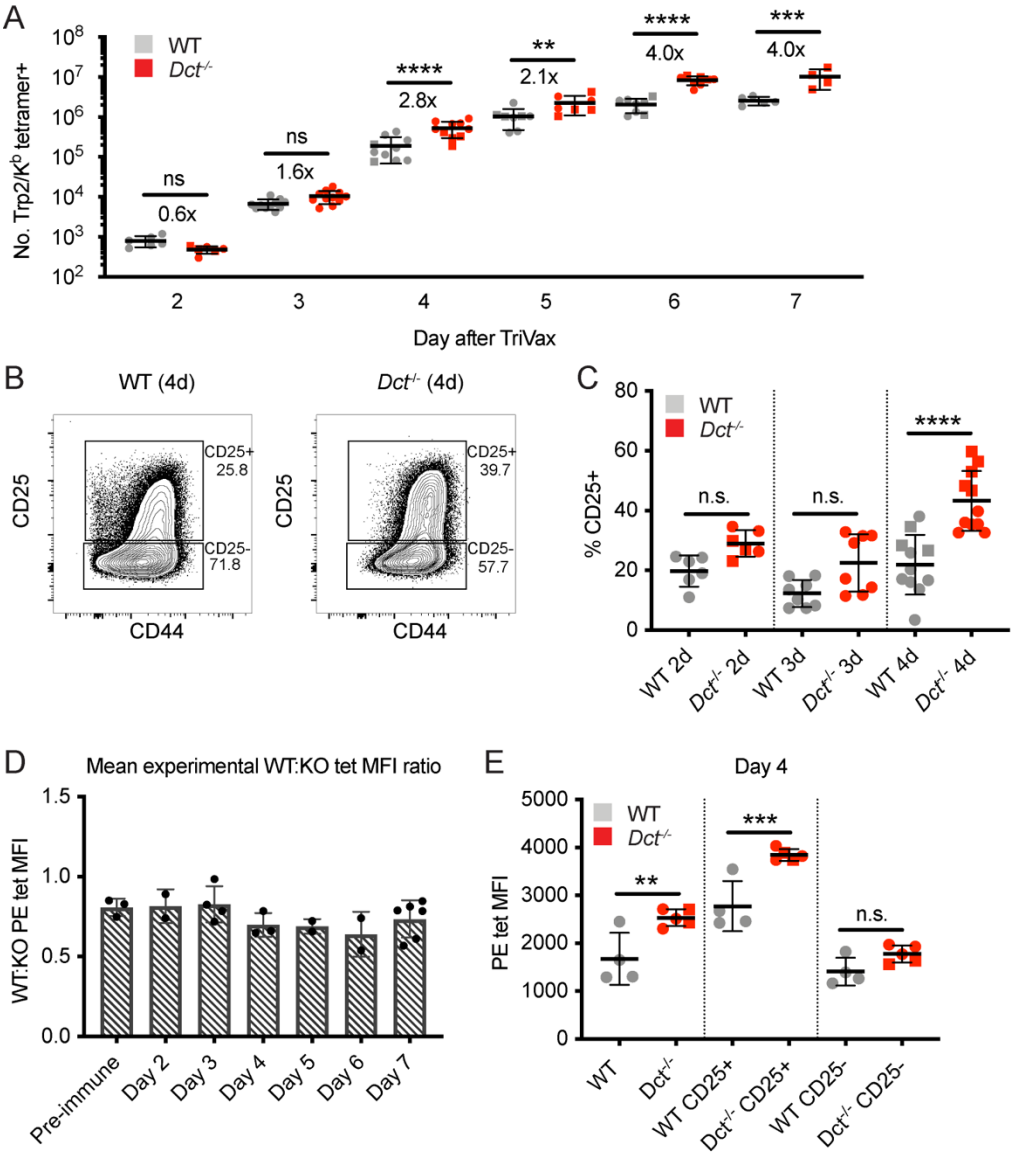

Figure 4. WT Trp2/K^b-specific cells are capable of an initial response to Trp2 similar to that of *Dct*$^{-/-}$ cells

WT and *Dct*$^{-/-}$ mice received intravenous injections of TriVax with 200 ug Trp2 peptide. Tetramer enrichment was used to enumerate Trp2/K^b-specific cells and assess their phenotype at the indicated time points following immunization (A–C, E). The ratio between the mean experimental PE MFI of Trp2/K^b-specific cells in WT mice relative to *Dct*$^{-/-}$ mice is plotted in D, with each symbol representing one experiment. Data are compiled from three or more experiments in A, D, and D. Representative flow plots from one day four experiment are shown in B, and the same representative day four experiment is shown in E. Squares indicate male animals; the dotted line indicates the average naïve precursor frequency from the spleen and lymph nodes. * $p < 0.05$, ** $p < 0.01$, *** $p < 0.001$, **** $p < 0.0001$ by one-way ANOVA with Sidak's multiple comparisons test (performed on log-transformed data in [a]).

We also assessed the phenotype of responding Trp2/K^b-specific cells acutely after TriVax. With this approach, CD69 did not serve as a reliable indicator of activation due to the type I interferon response induced by poly(I:C) leading to CD69 upregulation (Shiow et al., 2006), and widespread CD44 expression was seen in both tetramer positive and negative cells because of the potent inflammatory response unleashed by this method of immunization. Accordingly, we tracked CD25 expression as an indicator of activation. CD25, the high affinity alpha component of the IL-2 receptor, is upregulated with activation in certain situations (Valenzuela et al., 2002) and may enable a stronger effector response by cells expressing it (Obar et al., 2010). The proportion of Trp2/K^b-specific cells expressing CD25 was significantly greater in *Dct*$^{-/-}$ mice on day four, and trended higher on days two and three (Figure 4B, 4C). The CD25 MFI of CD25+ cells was also higher on *Dct*$^{-/-}$ Trp2/K^b-specific cells on day four (Figure 4B), suggesting that *Dct*$^{-/-}$ cells expressed more CD25 on a per-cell basis. Once again, *Dct*$^{-/-}$ Trp2/K^b-specific cells displayed significantly higher tetramer MFI than WT cells on days two through seven, but the avidity differences detected by tetramer staining did not demonstrate a progressive increase with time; the ratio between the WT and *Dct*$^{-/-}$ tetramer MFI transiently dropped at days 4–6, but the ratio at day 7 was similar to that of pre-immune cells (Figure 4D, S3A). Tetramer MFI was highest among the CD25+ subset for both WT and *Dct*$^{-/-}$ cells; the tetramer MFI of CD25+ WT cells was similar to the MFI of the overall tetramer-binding *Dct*$^{-/-}$ population on day four (Figure 4E).

We also assessed the early response following peptide stimulation alone, since this would be analogous to encountering Trp2 in a non-inflammatory context. We again found the early response to be similar between WT and *Dct*$^{-/-}$ Trp2/K^b-specific cells. The number (Supplemental figure 3B) and phenotype of WT Trp2/K^b-specific cells was comparable to that of *Dct*$^{-/-}$ cells on day one post-peptide. The activation markers CD44 and CD69 were similarly upregulated in both (Supplemental figure 3C, 3D), however, responses began to diverge by day two after peptide stimulation, and by day three significant differences in number and CD44 expression had emerged, with *Dct*$^{-/-}$ cells clearly outperforming WT cells (Supplemental figure 3B, 3C).

These findings indicate that the response to Trp2/K^b in WT and *Dct*$^{-/-}$ mice follows similar kinetics and magnitude but that expansion in WT animals terminates prematurely. Interestingly, we did not observe a progressive increase in apparent TCR avidity over time among the *Dct*$^{-/-}$ responder pool relative to WT cells, as might be expected if the subset of *Dct*$^{-/-}$ T cells with higher avidity TCRs became more dominant in the response to Trp2/K^b.

Single-cell sequencing reveals an impaired ability to differentiate into a highly proliferative population among WT Trp2/K^b-specific cells

To better understand the defects in expansion and functionality observed among WT Trp2/K^b-specific cells and assess the heterogeneity within this population, we performed single-cell RNA sequencing on Trp2/K^b-specific cells from WT and *Dct*$^{-/-}$ mice at day three after TriVax priming. After initial data processing, the WT and *Dct*$^{-/-}$ datasets were merged (Stuart et al., 2019); clusters based on the cells' transcriptomes were generated

in an unbiased manner and visualized using uniform manifold approximation and projection (UMAP). Cells clustered into two major groups separated along the x-axis, each comprised of smaller clusters (Figure 5A). Interestingly, over half of the cells (58%) from *Dct*$^{-/-}$ mice were localized in cluster 0, but this cluster was nearly devoid of WT cells, representing only a small subset (13%) of WT cells (Figure 5B). Suspecting that this cluster might contain a more functional subset poorly represented in the WT population, we assessed its characteristics in more detail. Because this cluster made up the majority of Group A (left group), we performed differential gene expression analysis between the two major groups in the merged dataset: A and B (right group).

Histone genes (e.g., *Hist1h1b*, *Hist1h1e*, *Hist1h1d*, *Hist2h2ac*) were among the most upregulated in Group A compared to Group B; these genes are commonly induced in association with cellular replication (Mei et al., 2017). Other genes associated with proliferation, such as *Myc*, *Nolc1*, *Npm1*, and *Ccne2*, were also upregulated in Group A (Figure 5C), and cell cycle analysis revealed that the majority of cells in Group A were in stages G2/M or S of the cell cycle (Figure 5D). Among cells in cluster 0 (Group A), 76% of *Dct*$^{-/-}$ cells were in G2/M or S versus 42% of WT cells (Figure 5E). Gene set enrichment analysis revealed a strong enrichment of gene sets comprising Myc targets, E2F targets, and genes related to mTORC1 signaling and the G2/M checkpoint (Supplemental figure 4A).

Many of the cells in Group A expressed CD25, with the majority of the remainder located in cluster 2 of Group B (Figure 5F); cells in these clusters also showed enrichment for a gene signature associated with IL-2 receptor signaling (Supplemental figure 4B). This aligns with our finding that the frequency of cells expressing CD25 was greater in *Dct*$^{-/-}$ than WT Trp2/K^{b}-specific effectors (Figure 4C). Indeed, group A cells showed significantly higher expression of certain genes relevant to the IL-2 signaling pathway with known impacts on T cell function, such as *Irf4* and *Myc*; previous work has demonstrated that signaling through the IL-2 receptor is important for sustained *Myc* expression (Preston et al., 2015). Based on these data, we administered IL-2 complex (IL-2 + anti-IL-2 S4B6 antibody) treatment to WT and *Dct*$^{-/-}$ mice previously primed with TriVax to determine whether this would correct the defective proliferation of the WT Trp2/K^{b}-specific cells. IL-2 complex acts through the β and γ components of the IL-2 receptor, negating the impact of differential CD25 expression. IL-2 complex treatment on day five after TriVax or LmTrp2 improved the expansion of both WT and *Dct*$^{-/-}$ Trp2/K^{b} specific cells to a similar extent (Supplemental figure 4C, 4D). Although this treatment did not correct the expansion defect of WT Trp2/K^{b}-specific cells in a selective manner, it did improve their numbers to the level seen among untreated *Dct*$^{-/-}$ cells, supporting the use of IL-2R-directed therapies in cancer immunotherapy designed to engage tolerant cells (Moynihan et al., 2016; Rosenberg, 2014; Waithman et al., 2008).

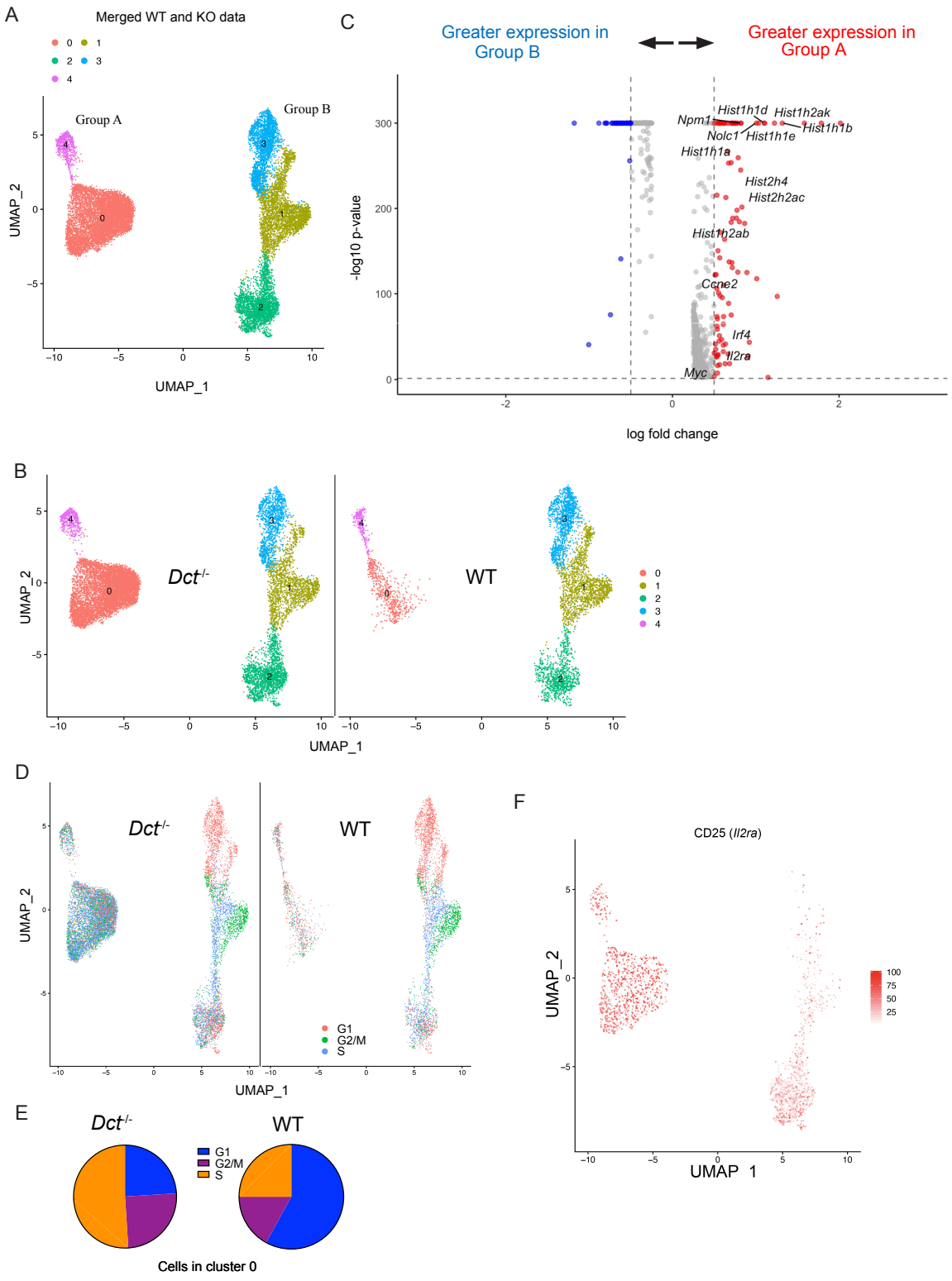

380

Figure 5. WT Trp2/K^b-specific cells show proliferative defects in the early effector phase
Trp2/K^b-specific CD8+ T cells were isolated from WT and *Dct*$^{-/-}$ mice on day three after TriVax and submitted for scRNA-seq. After initial processing, the WT and *Dct*$^{-/-}$ data sets were merged and further analyzed. (A) UMAP representation of gene expression from merged datasets determined using Seurat; each dot represents one cell. Clusters are indicated by color. (B) Cells from the *Dct*$^{-/-}$ sample are shown on the left and cells from the WT sample on the right using the same UMAP projection (generated from merged data) shown in Fig. 6A. (C) The most differentially expressed genes between groups A and B (see Fig. 6A); histone genes and other genes associated with proliferation are indicated. A positive average log fold change value indicates higher expression in group A. (D) Cell cycle analysis indicates the cell cycle phase for each cell on the UMAP plot (cells from the *Dct*$^{-/-}$ sample are shown on the left and cells from the WT sample on the right). (E) Pie charts show the frequencies of cells within cluster 0 in each stage of the cell cycle (left: *Dct*$^{-/-}$ sample, right: WT sample). (F) Expression of CD25 (*Il2ra*) by cell is indicated on the clusters by color.

Taken as a whole, the RNA-sequencing data suggest that WT Trp2/K^b-specific cells are deficient in their ability to form the more proliferative subpopulation that comprises a majority of the *Dct*$^{-/-}$ Trp2/K^b-specific population on day three after priming. Nevertheless, proliferation of the WT population was not entirely constrained, since this pool continued to expand over successive days (Figure 4).

WT Trp2/K^b-specific cells are inefficient at mediating vitiligo

T cells that escape self-tolerance mechanisms can sometimes elicit autoimmunity. Even CD8$^+$ T cells with very low affinity TCRs that avoid deletional tolerance have been found to drive tissue destruction following activation (Enouz et al., 2012; Sabatino et al., 2011; Zehn & Bevan, 2006). Furthermore, vigorous immunization against Trp2 can break tolerance and lead to vitiligo (Bowne et al., 1999; Cho & Celis, 2009; Moynihan et al., 2016). Our data indicated that the proliferative response of Trp2/K^b-specific cells was only slightly impaired in WT relative to *Dct*$^{-/-}$ mice, but the ability of these expanded cells to mediate overt tissue damage, as indicated by autoimmune vitiligo, was unclear.

To investigate this, we primed WT and *Dct*$^{-/-}$ donors with TriVax, then transferred day seven effectors to congenically distinct WT recipient mice in parallel and immunized these recipients with TriVax. Equal numbers of *Dct*$^{-/-}$ and WT cells were transferred to compensate for the reduced response in WT mice. The recipients were treated with dinitrofluorobenzene (DNFB) on the left flank six days after transfer as a local inflammatory stimulus (Haas et al., 1992; Mackay et al., 2012; Zhang et al., 2009); vehicle (acetone/olive oil) was applied to the right flank (Figure 6A). Analysis of the blood six days after transfer and boosting revealed expansion of both types of donor cells; although there was a trend for transferred *Dct*$^{-/-}$ cells to expand to a greater degree than donor WT cells, the difference was not statistically significant (Figure 6B). Recipient mice were subsequently monitored for vitiligo development on a weekly basis and scored using a numeric metric (Supplemental figure 5A).

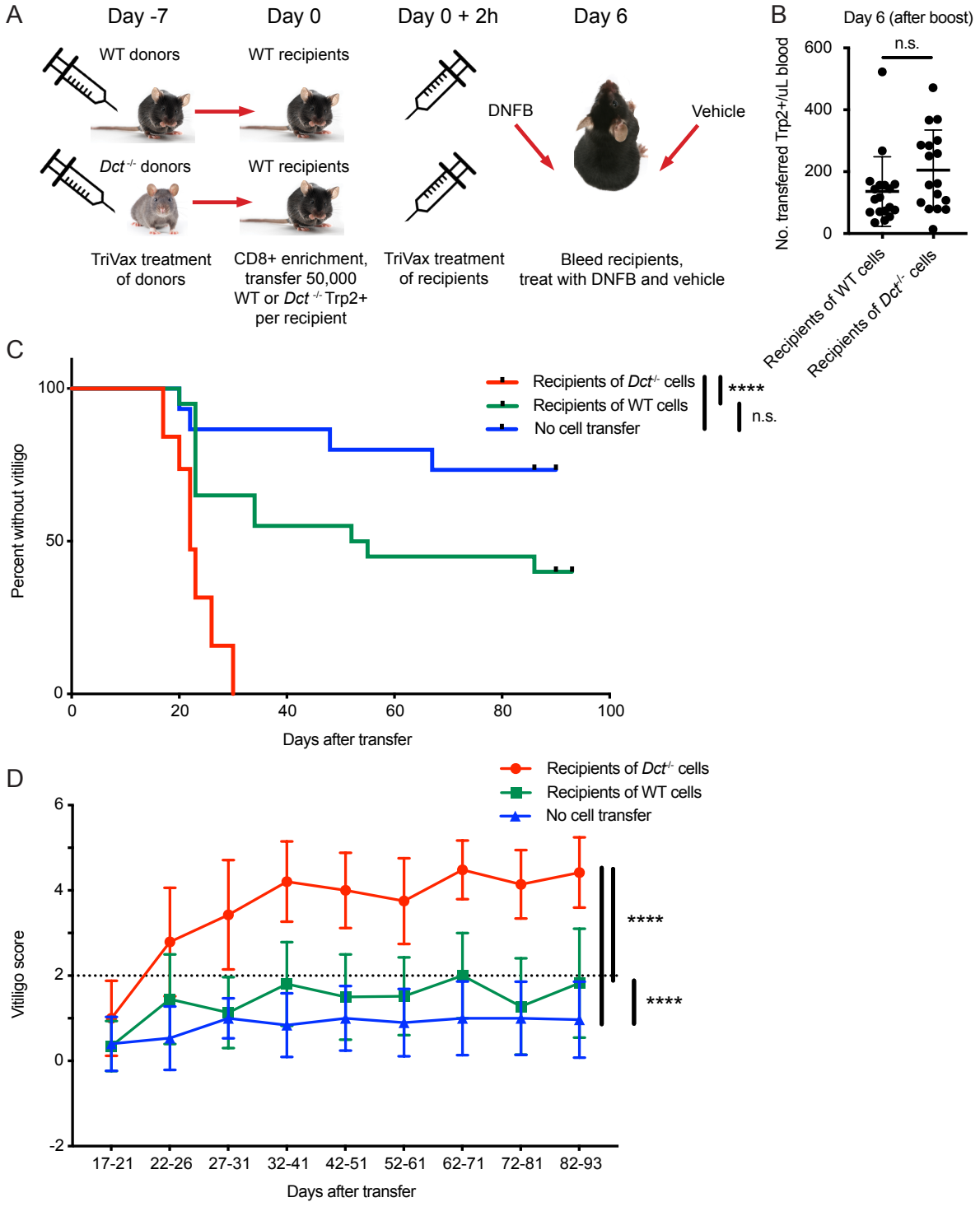

Figure 6. WT Trp2/K^b-specific cells are unable to mediate efficient anti-melanocyte activity
(A) WT mice were monitored for vitiligo after receiving 50,000 Trp2/K^b-specific cells from WT or *Dct*$^{-/-}$ donors primed with TriVax seven days prior; recipient mice received TriVax (100 ug Trp2) on the day of transfer and were treated with DNFB (left flank) six days later. No cell transfer controls (not shown in schematic) received TriVax and DNFB but no transferred cells. (B) Recipient mice were bled on day six after transfer and TriVax; the number of transferred Trp2/K^b-positive cells per uL blood is shown. (C) Kaplan Meier curve of vitiligo development; mice were considered to have vitiligo when they first had a vitiligo score of two that was sustained. Mean group vitiligo scores over time are shown in (D), with a dotted line indicating definite vitiligo. Data in C and D are compiled from three experiments with 4–10 mice per group. Data in B are compiled from two experiments with 4–10 mice per group. **** $p < 0.0001$ by unpaired t test (B), log-rank survival analysis (C), or two-way ANOVA followed by Tukey's multiple comparisons test (D).

Recipients of *Dct*$^{-/-}$ cells developed vitiligo more rapidly and more extensively than mice receiving WT cells, beginning around day 20 after cell transfer (Figure 6C). Vitiligo was most frequently initiated at the DNFB-treated site and would often progress over the following weeks to involve the right flank, hair around the eyes, and—in some cases—hair distributed over the body. Vitiligo progressed more rapidly and to a greater extent (higher numeric score) in recipients of *Dct*$^{-/-}$ cells (Figure 6D, Supplemental figures 5B and 5C), although low-grade vitiligo was observed in some mice receiving WT Trp2/K^b-specific effector cells or TriVax and DNFB without cell transfer. It is possible that initial melanocyte destruction mediated by the transferred cells facilitated antigen release and a broadening of the anti-melanocyte response to include endogenous T cells; nevertheless, preliminary studies using irrelevant TCR transgenic mice (P14) as recipients showed that Trp2/K^b-specific donor cells from *Dct*$^{-/-}$ mice were still able to induce vitiligo in this setting (data not shown).

Vitiligo severity (average vitiligo score) was positively correlated with the number of donor Trp2/K^b-specific cells in the blood on day 6 after transfer and TriVax boost (Supplemental figure 5D). This suggests that the enhanced proliferative capacity of *Dct*$^{-/-}$ cells was a factor in their superior ability to induce vitiligo, although it does not rule out additional qualitative differences between the WT and *Dct*$^{-/-}$ populations.

In summary, in contrast to the relatively modest differences in the expansion of Trp2/K^b responders in WT and *Dct*$^{-/-}$ mice, the ability of these populations to mediate autoimmune damage—melanocyte destruction—was strikingly different.

Discussion

A number of groups have demonstrated the existence of self-reactive CD8+ and CD4+ T cells in the periphery of mice and healthy human adults (Anderson et al., 2000; Bloom et al., 1997; Delluc et al., 2010; Maeda et al., 2014; Su et al., 2013; Yu et al., 2015). In some cases, self-reactive cells display indicators of reduced functionality, revealing them as tolerant and unlikely to cause spontaneous pathology. For example, self-reactive cells are often reported to express inhibitory receptors such as CTLA-4, PD-1, and LAG-3 (Fife & Bluestone, 2008; Maeda et al., 2014; Nelson et al., 2019; Schietinger et al., 2012). However, studies in human adults have identified self-reactive cells with a phenotype similar to that of naïve CD8+ T cells specific for foreign antigens (Yu et al., 2015); these cells did not display an overtly anergic phenotype but still responded poorly to stimulation. It is important to understand the mechanisms restraining these cells under normal conditions as well as their potential to cause pathology; such knowledge is critical to designing effective therapies to restrain these cells (e.g., to control autoimmune disease) or induce their responses (e.g., for cancer immunotherapy). As described in this report, we developed a polyclonal mouse model for non-deletional self-tolerance, enabling us to define the characteristics of these cells and their reactivity in a physiological setting.

We found that the pre-immune population of Trp2/K^b-specific cells in WT and *Dct*$^{-/-}$ strains were qualitatively similar, sharing a naïve phenotype and indistinguishable gene expression profile; there were no clear signs of prior antigen exposure among the WT cells. The size of the Trp2/K^b-specific precursor pool was only slightly (although significantly) smaller in WT mice and the response to Trp2 immunization was substantial in both strains, leading to a > 1000-fold expansion of Trp2/K^b-specific cells in both WT and *Dct*$^{-/-}$ mice. Despite these commonalities, cells primed in *Dct*$^{-/-}$ mice proliferated more extensively and were capable of much more rapid and widespread tissue destruction, read out as vitiligo, after adoptive transfer.

Our adoptive transfer studies showed that the observed restraint in the WT Trp2/K^b-specific response did not depend on extrinsic factors but was a cell-intrinsic feature of pre-immune $CD8^+$ T cells. This implies that other cell populations, including CD4+ Tregs or regulatory CD8+ T cells (Saligrama et al., 2019) are neither required for nor capable of affecting the responses of tolerant and non-tolerant Trp2/K^b-specific cells during priming. These findings also effectively eliminate the possibility that self-antigen presentation during Trp2 priming alters the nature of the immune response. However, while our studies argue that cell-extrinsic regulation is not required for enforcement or maintenance of tolerance by Trp2/K^b-specific cells, this does not exclude a potential role for regulatory T cell populations in establishing the initial tolerant state in WT mice. It is currently unclear whether tolerance to Trp2 is enforced during thymic development or in the periphery of WT mice: one report suggested that *Dct* expression is undetectable in thymic mTECs (Träger et al., 2012), but Trp2 could be brought into the thymus by dendritic cell populations to induce tolerance in WT animals. The site of tolerance induction was not a focus of the current study, but it will be interesting to determine whether instances of non-deletional $CD8^+$ T cell self-tolerance correlate with self-

antigen expression patterns in the thymus (e.g., AIRE-regulated tissue-specific antigen expression).

Many of the characteristics we report for Trp2/K^b-specific $CD8^+$ T cells in WT mice are strongly reminiscent of T cells with low affinity/avidity for antigen (Bouneaud et al., 2000; Enouz et al., 2012; Zehn & Bevan, 2006; Zehn et al., 2009), and we did observe modestly higher Trp2/K^b tetramer staining intensity on a subset of *Dct*$^{-/-}$ cells compared to WT responder cells. However, these differences were not progressively magnified as the immune response developed, arguing against a noticeable outgrowth of higher affinity/avidity TCR clones in *Dct*$^{-/-}$ animals, as might have been expected if TCR affinity was the primary factor driving improved proliferation in the *Dct*$^{-/-}$ population. Indeed, the relatively subtle differences in Trp2/K^b tetramer staining that we were able to detect in this optimized experimental model would not likely be sufficient to predict self-reactivity versus tolerance in a less controlled setting.

Other studies utilizing mouse models have reported that even $CD8^+$ T cells with very low affinity/avidity TCRs (including those undetectable by normal peptide/MHC tetramer staining) can provoke overt tissue damage (Enouz et al., 2012; Sabatino et al., 2011; Zehn & Bevan, 2006), in some cases at levels comparable to or greater than that induced by non-tolerant and/or higher affinity cells. Our data indicate that the opposite can also occur: despite largely overlapping tetramer staining profiles, WT and *Dct*$^{-/-}$ Trp2/K^b-specific cells exhibit markedly different abilities to mediate widespread vitiligo. Hence, the impact of $CD8^+$ T cell tolerance toward some self-antigens only partially limits expansion but can prevent the generation of cells readily capable of potent tissue destruction: tolerance is not a binary state.

A goal of this work was to define which characteristics, if any, could be associated with self-tolerant $CD8^+$ T cells that escape clonal deletion. Unexpectedly, we found that multiple measures—the enumeration, peptide/MHC tetramer staining intensity, phenotype, and gene expression of pre-immune cells as well as the ability of these cells to proliferate following immunogenic exposure to self-antigens—failed to provide a robust metric for distinguishing $CD8^+$ T cells that are functionally tolerant (i.e., unlikely to cause autoimmune pathology) versus non-tolerant (i.e., have a high propensity to induce autoimmunity). This finding highlights the limitations of currently available assays for accurately predicting responsiveness to self-antigens.

However, we were able to delineate an inflection point following priming at which the responses of tolerant and non-tolerant cells diverged. Flow cytometry and single-cell RNA sequencing of Trp2/K^b-specific $CD8^+$ T cells soon after priming demonstrated that WT responders failed to differentiate into a CD25+, IRF4+ population (a characteristic of most *Dct*$^{-/-}$ responder cells) and indicated that WT cells showed poor commitment to sustained proliferation. These combined features may be useful for further defining the responses by self-antigen specific cells that are or are not capable of overt tissue destruction.

The early effector population of Trp2/K^b-specific cells demonstrates heterogeneity on a transcriptomic level in both strains. Whereas the majority of *Dct*$^{-/-}$ cells show a highly proliferative phenotype characterized by active cell cycling and responsiveness to mTOR and Myc, few WT Trp2/K^b-specific cells fall into this group. The reason(s) underlying the inability of WT cells to optimally engage these important pathways and proliferate efficiently requires further investigation but may relate to impaired sensitivity to endogenous IL-2 or other cytokines, the composition of the TCR repertoire, and/or altered TCR signaling. How these or other factors relate to the relative inability of primed WT Trp2/K^b-specific cells to mediate overt tissue damage is currently unclear, but it will be critical to identify the cellular and molecular mechanisms involved in future studies. Ongoing and future work will address the TCR repertoire and downstream signaling, metabolic characteristics, and epigenetic landscape of WT versus *Dct*$^{-/-}$ Trp2/K^b-specific cells. Recent studies on dysfunctional tumor-specific or exhausted CD8+ T cells have shown that epigenetic changes in chromatin accessibility or methylation can maintain such states (Ghoneim et al., 2017; Pauken et al., 2016; Philip et al., 2017), which could explain the cell-intrinsic nature of the tolerance seen in our model.

We were able to identify CD8+ T cells specific for other melanocyte epitopes/antigens in pre-immune mice; these cells had a similar phenotype to WT Trp2/K^b-specific cells. Accordingly, we predict that our results will apply to other populations of CD8+ T cells specific for melanocyte and potentially other tissue-restricted antigens. Similar populations of self-specific $CD8^+$ T cells may exist in humans, and the ability of such cells to respond to self-antigen immunization while not causing autoimmune damage is relevant for understanding the limits of “breaking” tolerance, e.g., for cancer immunotherapy. Indeed, our results align with work examining polyclonal self-antigen-specific cells in human adults (Yu et al., 2015) with regard to the phenotype (modestly lower tetramer MFI, lower CD25 expression) and response to cognate peptide (diminished) observed among tolerant cells. Another study examining self-specific $CD8^+$ T cells (Maeda et al., 2014) attributed their restrained responsiveness to Treg-mediated suppression; while we did not detect a cell-extrinsic regulatory mechanism in our studies, it is certainly possible that this mechanism limits the response to some self-antigens.

Our finding that polyclonal melanocyte-specific cells exhibit covert cell-intrinsic tolerance characterized by a partial defect in proliferation and a profound defect in tissue damage has implications for utilizing such cells therapeutically. This model has clear relevance to human physiology and will be useful in exploring methods of correcting the proliferative defects of tolerant cells to more effectively mobilize them in cancer immunotherapy approaches targeting tumor antigens shared with self.

Materials and methods

Mice

C57BL/6 (WT) mice were obtained from Charles River laboratories and housed in specific pathogen-free conditions at the University of Minnesota. *Dct*$^{-/-}$ mice on a C57BL/6 background were developed by A. Andy Hurwitz when at the NCI; the mice were subsequently bred in-house on different congenic backgrounds and housed in specific pathogen-free conditions. Animals were used at 6–14 weeks of age. All animal experiments were approved by the Institutional Animal Care and Use Committee at the University of Minnesota. In accordance with NIH guidelines, both male and female animals were used in experiments; males are indicated by square symbols in the figures.

Tetramer enrichment

Tetramer enrichment was used to isolate antigen-specific cells from pre-immune or acutely challenged mice. A modification of the method used by Obar et al. (Obar et al., 2008) was employed. Following digestion with collagenase D, single-cell suspensions were prepared from the spleens (acutely challenged mice) or spleen and peripheral/mesenteric lymph nodes (pre-immune mice). When possible, the same tetramer ($Trp2_{180–188}/K^b$) was used in both APC and PE to ensure specificity. Anti-PE and anti-APC beads and magnetized columns (both from Miltenyi Biotec) were used to enrich for tetramer-bound cells. Samples were stained and analyzed by flow cytometry; CountBright counting beads (Invitrogen) were used for enumeration.

In vivo priming with Trp2

TriVax immunization was used as previously described (Cho & Celis, 2009); mice were immunized intravenously (via tail vein injections) with $Trp2_{180–188}$ peptide or Trp2 and $B8R_{20–27}$ peptides, agonist-anti CD40 antibody (BioXCell), and vaccine-grade poly(I:C), a toll-like receptor 3 agonist (InvivoGen). Peptide doses of 50, 100, and 200 μg were used for effector timepoints, transfer experiments, and acute timepoints, respectively. Animals that received TriVax immunization via intraperitoneal instead of intravenous injection were removed from the analysis.

Infections with LmTrp2

Frozen stocks of LmTrp2 (Bruhn et al., 2005) were thawed and grown to log-phase in tryptic soy broth supplemented with streptomycin (50 μg/mL). Mice were typically injected with approximately 10^5–10^6 colony-forming units intravenously or intraperitoneally. Infectious doses were verified by colony counts on tryptic soy broth-streptomycin plates.

Ex vivo stimulation

In some experiments, splenocytes were stimulated ex vivo after isolation from infected mice. Splenocytes were incubated with Trp2 peptide (10^{-6} M) and Golgiplug (BD Biosciences) for 4–6 hours at 37°C; parallel wells with no peptide were used as a control. Cells were washed and stained with surface antibodies, followed by fixation and

permeabilization with a FoxP3 Fix/Perm kit (eBioscience) or FoxP3/transcription factor staining buffer kit (Tonbo Biosciences) and staining with intracellular antibodies.

Adoptive transfer experiments

Bulk polyclonal CD8+ T cells were isolated from the spleen and lymph nodes of WT or *Dct*$^{-/-}$ mice using negative magnetic enrichment (CD8a+ T cell Isolation Kit; Miltenyi Biotec). Enriched CD8+ T cells (typically ~75-90% pure) were resuspended in sterile PBS and 2–2.5 x 10^6 CD8+ T cells were injected intravenously per recipient mouse; recipient mice were congenically distinct. One day later, the recipient mice were immunized with TriVax or LmTrp2 intravenously or intraperitoneally. Mice were sacrificed for analysis seven days later.

Bulk RNA sequencing of pre-immune mice

Trp2/K^b-specific cells were isolated from pre-immune WT and *Dct*$^{-/-}$ mice using tetramer enrichment followed by fluorescence-activated cell sorting on double tetramer positive cells. Cells were isolated from three separate cohorts, with each cohort comprising eight WT and eight *Dct*$^{-/-}$ mice. The Clontech StrandedRNA Pico Mammalian workflow was used for library preparation, and samples were sequenced using an Illumina NextSeq instrument (2x75 bp paired end reads).

Bulk RNAseq analysis

Raw sequencing data were demultiplexed by sample into FASTQs (mean 24.6 million reads/sample) and mapped against the mouse genome (Ensembl GRCm38 release 95) using Hisat2 software (v 2.1.0). Gene level quantification was completed using Subread featureCounts software (v 1.6.2) and the read counts table was processed in R (v 3.5.2). Differentially expressed genes were identified with DESeq2 software (v 1.22.2) using a negative binomial model with effect size estimation completed by apeglm algorithm via the lfcShrink function. Group comparison p-values were adjusted by the Benjamini and Hochberg method to account for multiple hypothesis testing where genes with a false discovery rate (FDR) $q < 0.05$ were investigated in downstream analyses.

Single-cell RNA sequencing

WT and *Dct*$^{-/-}$ mice were primed with TriVax (200 μg Trp2), and Trp2/K^b-specific cells were isolated on day three using tetramer enrichment followed by fluorescence-activated cell sorting. Cells were submitted for barcoding and library preparation using the 10x Genomics platform (Chromium Single Cell 5' Library & Gel Bead Kit) (Zheng et al., 2017) and each sample was sequenced using an Illumina NovaSeq instrument with 2x150 bp paired end protocol.

Single-cell RNAseq analysis

Raw sequencing data were processed using Cell Ranger (v 3.0.2; 10x Genomics) software programs "mkfastq" for demultiplexing the WT and *Dct*$^{-/-}$ Illumina libraries and "count" for read alignment against the mouse genome (mm10, provided by 10x Genomics, ver 3.0.0) and generation of the mRNA transcript count table. Raw count data were loaded into R (v 3.6.1) and analyzed with the Seurat R package (v

3.0.3.9039) (Butler et al., 2018; Stuart et al., 2019). Each scRNA dataset (WT or *Dct*$^{-/-}$) was independently filtered to include only cells (i.e. uniquely barcoded transcripts) expressing more than 300 genes and genes expressed in more than 3 cells (e.g. counts > 0). The proportion of mitochondrial RNA in each cell was calculated and cells with extreme levels (top or bottom 2% of all cells) were removed from the analysis. Genes with extreme expression levels (top or bottom 1% of all genes) were removed. Contaminating cells expressing high levels of B cell or myeloid lineage marker genes and low levels of T cell markers were removed using empirically derived thresholds (675 B cells and 26 myeloid cells removed from WT and 117 B cells removed from *Dct*$^{-/-}$). A total of 4,539 WT cells (19,326 genes) and 11,680 *Dct*$^{-/-}$ cells (19,416 genes) were analyzed downstream. Raw RNA counts were normalized with the LogNormalize function and each cell was classified according to its expression of canonical cell cycle genes using the CellCycleScoring function (gene sets provided in Seurat). Raw RNA counts were normalized and transformed using the Seurat SCTransform function (Hafemeister & Satija, 2019) including the percent of mitochondria expression and cell cycle S/G2M-phase scores as regression factors. Principal components analysis (PCA) was performed using the normalized, mean-centered, and scaled SCT dataset (RunPCA function). The top 3000 variable genes from each dataset were identified using the FindVariableFeatures function (vst method) and were used for WT and *Dct*$^{-/-}$ sample integration (Stuart et al., 2019). Two-dimensional projections were generated using the top 30 PCA vectors as input to the RunTSNE and RunUMAP functions. Cells were clustered using the FindNeighbors (top 30 PCA vectors) and FindClusters functions (testing a range of possible resolutions: 0.2, 0.4, 0.8, 1.2, 1.6). Pairwise differential gene expression (DE) testing (Wilcox rank-sum) with the FindMarkers function was performed between all initial clusters; any two clusters were merged if there were fewer than 5 significant DE genes (i.e. absolute value of log2-fold-change >= 0.25 and Bonferroni adjusted p-value <= 0.01). Pairwise DE testing continued on subsequently merged clusters. A final resolution of 0.2 was chosen (merging of initial clusters by DE testing was not required) to best represent the biological processes within the dataset. Cluster-specific pathway expression testing was completed using the VISION R package (DeTomaso et al., 2019) and figures were generated using the ggplot2 R package (Wickham, 2016). Gene Set Enrichment Analysis (Mootha et al., 2003; Subramanian et al., 2005) was performed using pre-ranked gene lists (sorted from largest to smallest log2 fold change between clusters compared). Gene set enrichment statistics were calculated for two gene set collections in the Molecular Signatures Database (hallmarks and c2 curated) derived for mouse symbols using the R package msigdbr, v 6.2.1 using the R package clusterProfiler (v 3.12.0). Interesting gene sets with a FDR q < 0.05 were evaluated. Raw and processed data have been deposited at Gene Expression Omnibus and are available via GEO.

IL2 complex treatment

10 μg antibody (S4B6-1; Bio XCell) plus 1 ug murine recombinant carrier-free murine IL-2 (R&D) was administered per mouse via intraperitoneal injection on day 5 after priming with TriVax or LmTrp2; control mice received an equal volume of PBS.

Vitiligo induction

Donor mice (WT and *Dct*$^{-/-}$) were primed with TriVax (100 μg Trp2); in one experiment, donor mice received ~50% less of the other TriVax components to minimize adverse reactions. Negative enrichment for CD8+ T cells was performed on day seven. Live cells were counted using a hemocytometer, and the percentages of CD8+ and Trp2/K^{b} tetramer-binding cells were applied to enumerate Trp2/K^{b}-specific cells; equal numbers (50,000) of WT or *Dct*$^{-/-}$ Trp2/K^{b}-specific cells were transferred to WT recipients. Recipients were treated with TriVax (100 μg Trp2) later the same day. On day six after cell transfer, the recipients were bled to assess donor populations. The mice were then treated with dinitrofluorobenzene (DNFB; 0.15% in 4:1 acetone:olive oil) on the left flank; 30 μL was applied to a shaved patch of skin ~ 1.5 x 1.5 cm in size. 30 μL of vehicle was applied to the right flank in the same manner. Control mice did not receive cell transfers, but did receive TriVax immunization and DNFB treatment at the same time as mice receiving cell transfers. Mice were monitored for vitiligo development on a weekly basis by an observer blinded to the experimental groups.

Tetramers and flow cytometry

H-2K^{b} tetramers loaded with Trp2$_{180\text{-}188}$ or B8R$_{20\text{-}27}$ were obtained from the NIH tetramer core facility and labelled with streptavidin-fluorophore conjugates in house. Single-cell suspensions were stained with tetramers (when applicable) and fluorescent dye-conjugated antibodies purchased from BD Biosciences, Tonbo Biosciences, eBioscience, or BioLegend. In many experiments, Live/Dead Fixable Aqua Dead Cell Stain Kit (ThermoFisher Scientific) was used for dead cell exclusion. When applicable, cells were fixed with a FoxP3 Fix/Perm kit (eBioscience) or FoxP3/transcription factor staining buffer kit (Tonbo Biosciences). These kits were also used for permeabilization prior to staining with intracellular antibodies. Samples were run on a BD LSR II or BD Fortessa instrument using BD FACSDiva (BD Bioscience), and data were analyzed with FlowJo (BD).

Statistical analysis

Prism software (GraphPad) was used to plot data and conduct statistical analyses. An unpaired t test was used for two-way comparisons between two groups. A one-way ANOVA with Sidak's or Tukey's multiple comparisons test was used when multiple comparisons were performed. Log-rank (Mantel-Cox) tests were used to evaluate Kaplan-Meier curves. A two-way ANOVA with Tukey's multiple comparisons test was used to evaluated vitiligo scores over time. P-values are represented as follows: * $p < 0.05$, ** $p < 0.01$, *** $p < 0.001$, **** $p < 0.0001$.

Supplemental material

Fig. S1 shows additional analysis of the Trp2/K^{b}-specific population and cells specific for other melanocyte epitopes in pre-immune mice. Fig. S2 presents data using LmTrp2 as an alternative method of stimulating with Trp2. Fig. S3 shows overlays of tetramer staining at various time points after TriVax immunization, along with the acute response to in vivo stimulation with Trp2 peptide alone. Gene set enrichment analysis of single-

cell data and the response of WT and KO Trp2/K^b-specific cells to IL-2C are presented in Fig. S4. Fig. S5 shows the vitiligo scoring metric and correlation analysis of the average vitiligo score relative to the number of transferred Trp2/K^b-specific cells following transfer and boosting.

Author contributions

ENT, KRR, and SCJ designed experiments and interpreted results. ENT, KSB, HBdS, KEB, and KRR performed experiments, and ENT analyzed results. TPK performed bioinformatics analysis of RNAseq data and wrote the relevant portions of the Methods section. AAH and KRS created the *Dct*-deficient mouse strain. RBF performed initial experiments leading to these studies and provided guidance. ENT and SCJ wrote the manuscript, with all authors contributing to edits.

Acknowledgments

We thank members of the Jamequist lab for helpful discussions and technical assistance. We thank the UMN Flow Cytometry Resource for cell sorting, the UMN Genomics Center for assistance with sequencing experiments, and the NIH tetramer core for peptide/MHC monomers. We thank the Celis and Restifo labs for providing reagents and samples used in enumerating cells specific for alternative melanocyte epitopes. We thank Dietmar Zehn for reviewing an early draft of this manuscript.

This work was supported by NIH grants P01 AI035296 (SCJ), R01 AI140631 (SCJ), and T32 OD010993 (ENT).

Competing interests

The authors declare no competing financial interests.

References

Anderson, A. C., Nicholson, L. B., Legge, K. L., Turchin, V., Zaghouani, H., & Kuchroo, V. K. (2000). High frequency of autoreactive myelin proteolipid protein-specific T cells in the periphery of naive mice: mechanisms of selection of the self-reactive repertoire. *J Exp Med, 191*(5), 761-770.

Avogadri, F., Gnjatic, S., Tassello, J., Frosina, D., Hanson, N., Laudenbach, M., . . . Jungbluth, A. A. (2016). Protein Expression Analysis of Melanocyte Differentiation Antigen TRP-2. *Am J Dermatopathol, 38*(3), 201-207. doi:10.1097/DAD.0000000000000362

Azzam, H. S., Grinberg, A., Lui, K., Shen, H., Shores, E. W., & Love, P. E. (1998). CD5 expression is developmentally regulated by T cell receptor (TCR) signals and TCR avidity. *J Exp Med, 188*(12), 2301-2311. doi:10.1084/jem.188.12.2301

Bloom, M. B., PerryLalley, D., Robbins, P. F., Li, Y., ElGamil, M., Rosenberg, S. A., & Yang, J. C. (1997). Identification of tyrosinase-related protein 2 as a tumor rejection antigen for the B16 melanoma. *Journal of Experimental Medicine, 185*(3), 453-459. doi:10.1084/jem.185.3.453

Bouneaud, C., Kourilsky, P., & Bousso, P. (2000). Impact of negative selection on the T cell repertoire reactive to a self-peptide: A large fraction of T cell clones escapes clonal deletion. *Immunity, 13*(6), 829-840. doi:10.1016/s1074-7613(00)00080-7

Bowne, W. B., Srinivasan, R., Wolchok, J. D., Hawkins, W. G., Blachere, N. E., Dyall, R., . . . Houghton, A. N. (1999). Coupling and uncoupling of tumor immunity and autoimmunity. *J Exp Med, 190*(11), 1717-1722.

Bruhn, K. W., Craft, N., Nguyen, B. D., Yip, J., & Miller, J. F. (2005). Characterization of anti-self CD8 T-cell responses stimulated by recombinant Listeria monocytogenes expressing the melanoma antigen TRP-2. *Vaccine, 23*(33), 4263-4272. doi:10.1016/j.vaccine.2005.02.018

Butler, A., Hoffman, P., Smibert, P., Papalexi, E., & Satija, R. (2018). Integrating single-cell transcriptomic data across different conditions, technologies, and species. *Nat Biotechnol, 36*(5), 411-420. doi:10.1038/nbt.4096

Byrne, K. T., Côté, A. L., Zhang, P., Steinberg, S. M., Guo, Y., Allie, R., . . . Turk, M. J. (2011). Autoimmune melanocyte destruction is required for robust CD8+ memory T cell responses to mouse melanoma. *J Clin Invest, 121*(5), 1797-1809. doi:10.1172/JCI44849

Cai, Z., Kishimoto, H., Brunmark, A., Jackson, M. R., Peterson, P. A., & Sprent, J. (1997). Requirements for peptide-induced T cell receptor downregulation on naive CD8+ T cells. *J Exp Med, 185*(4), 641-651.

Cheng, M., & Anderson, M. S. (2018). Thymic tolerance as a key brake on autoimmunity. *Nat Immunol, 19*(7), 659-664. doi:10.1038/s41590-018-0128-9

Cho, H. I., & Celis, E. (2009). Optimized Peptide Vaccines Eliciting Extensive CD8 T-Cell Responses with Therapeutic Antitumor Effects. *Cancer Research, 69*(23), 9012-9019. doi:10.1158/0008-5472.can-09-2019

832 Daniels, M. A., & Jameson, S. C. (2000). Critical role for CD8 in T cell receptor binding and
833 activation by peptide/major histocompatibility complex multimers. *J Exp Med, 191*(2),
834 335-346. doi:10.1084/jem.191.2.335

835 Daniels, M. A., Teixeiro, E., Gill, J., Hausmann, B., Roubaty, D., Holmberg, K., . . . Palmer, E.
836 (2006). Thymic selection threshold defined by compartmentalization of Ras/MAPK
837 signalling. *Nature, 444*(7120), 724-729. doi:10.1038/nature05269

838 Delluc, S., Ravot, G., & Maillere, B. (2010). Quantification of the preexisting CD4 T-cell
839 repertoire specific for human erythropoietin reveals its immunogenicity potential. *Blood,*
840 *116*(22), 4542-4545. doi:10.1182/blood-2010-04-280875

841 DeTomaso, D., Jones, M. G., Subramaniam, M., Ashuach, T., Ye, C. J., & Yosef, N. (2019).
842 Functional interpretation of single cell similarity maps. *Nat Commun, 10*(1), 4376.
843 doi:10.1038/s41467-019-12235-0

844 Enouz, S., Carrié, L., Merkler, D., Bevan, M. J., & Zehn, D. (2012). Autoreactive T cells bypass
845 negative selection and respond to self-antigen stimulation during infection. *J Exp Med,*
846 *209*(10), 1769-1779. doi:10.1084/jem.20120905

847 Fife, B. T., & Bluestone, J. A. (2008). Control of peripheral T-cell tolerance and autoimmunity via
848 the CTLA-4 and PD-1 pathways. *Immunol Rev, 224*, 166-182. doi:10.1111/j.1600-
849 065X.2008.00662.x

850 Fulton, R. B., Hamilton, S. E., Xing, Y., Best, J. A., Goldrath, A. W., Hogquist, K. A., & Jameson,
851 S. C. (2015). The TCR's sensitivity to self peptide-MHC dictates the ability of naive
852 CD8(+) T cells to respond to foreign antigens. *Nature Immunology, 16*(1), 107-+.
853 doi:10.1038/ni.3043

854 Ghoneim, H. E., Fan, Y., Moustaki, A., Abdelsamed, H. A., Dash, P., Dogra, P., . . .
855 Youngblood, B. (2017). De Novo Epigenetic Programs Inhibit PD-1 Blockade-Mediated T
856 Cell Rejuvenation. *Cell, 170*(1), 142-157.e119. doi:10.1016/j.cell.2017.06.007

857 Guyonneau, L., Murisier, F., Rossier, A., Moulin, A., & Beermann, F. (2004). Melanocytes and
858 pigmentation are affected in dopachrome tautomerase knockout mice. *Mol Cell Biol,*
859 *24*(8), 3396-3403. doi:10.1128/mcb.24.8.3396-3403.2004

860 Haas, J., Lipkow, T., Mohamadzadeh, M., Kolde, G., & Knop, J. (1992). Induction of
861 inflammatory cytokines in murine keratinocytes upon in vivo stimulation with contact
862 sensitizers and tolerizing analogues. *Exp Dermatol, 1*(2), 76-83. doi:10.1111/j.1600-
863 0625.1992.tb00075.x

864 Hafemeister, C., & Satija, R. (2019). Normalization and variance stabilization of single-cell RNA-
865 seq data using regularized negative binomial regression. *Genome Biol, 20*(1), 296.
866 doi:10.1186/s13059-019-1874-1

867 Hogquist, K. A., Baldwin, T. A., & Jameson, S. C. (2005). Central tolerance: Learning self-
868 control in the thymus. *Nature Reviews Immunology, 5*(10), 772-782. doi:10.1038/nri1707

869 Ji, Q., Gondek, D., & Hurwitz, A. A. (2005). Provision of granulocyte-macrophage colony-
870 stimulating factor converts an autoimmune response to a self-antigen into an antitumor
871 response. *J Immunol, 175*(3), 1456-1463. doi:10.4049/jimmunol.175.3.1456

872 Kappler, J. W., Roehm, N., & Marrack, P. (1987). T cell tolerance by clonal elimination in the
873 thymus. *Cell, 49*(2), 273-280. doi:10.1016/0092-8674(87)90568-x

874 Liu, H. P., Moynihan, K. D., Zheng, Y. R., Szeto, G. L., Li, A. V., Huang, B., . . . Irvine, D. J.
875 (2014). Structure-based programming of lymph-node targeting in molecular vaccines.
876 *Nature, 507*(7493), 519-+. doi:10.1038/nature12978

877 Mackay, L. K., Stock, A. T., Ma, J. Z., Jones, C. M., Kent, S. J., Mueller, S. N., . . . Gebhardt, T.
878 (2012). Long-lived epithelial immunity by tissue-resident memory T (TRM) cells in the
879 absence of persisting local antigen presentation. *Proc Natl Acad Sci U S A, 109*(18),
880 7037-7042. doi:10.1073/pnas.1202288109

881 Maeda, Y., Nishikawa, H., Sugiyama, D., Ha, D., Hamaguchi, M., Saito, T., . . . Sakaguchi, S.
882 (2014). Detection of self-reactive CD8(+) T cells with an anergic phenotype in healthy
883 individuals. *Science, 346*(6216), 1536-1540. doi:10.1126/science.aaa1292

884 McWilliams, J. A., McGurran, S. M., Dow, S. W., Slansky, J. E., & Kedl, R. M. (2006). A
885 modified tyrosinase-related protein 2 epitope generates high-affinity tumor-specific T
886 cells but does not mediate therapeutic efficacy in an intradermal tumor model. *J*
887 *Immunol, 177*(1), 155-161. doi:10.4049/jimmunol.177.1.155

888 Mei, Q., Huang, J., Chen, W., Tang, J., Xu, C., Yu, Q., . . . Li, S. (2017). Regulation of DNA
889 replication-coupled histone gene expression. *Oncotarget, 8*(55), 95005-95022.
890 doi:10.18632/oncotarget.21887

891 Mescher, M. F., Agarwal, P., Casey, K. A., Hammerbeck, C. D., Xiao, Z. G., & Curtsinger, J. M.
892 (2007). Molecular basis for checkpoints in the CD8 T cell response: Tolerance versus
893 activation. *Seminars in Immunology, 19*(3), 153-161. doi:10.1016/j.smim.2007.02.007

894 Mootha, V. K., Lindgren, C. M., Eriksson, K. F., Subramanian, A., Sihag, S., Lehar, J., . . .
895 Groop, L. C. (2003). PGC-1alpha-responsive genes involved in oxidative
896 phosphorylation are coordinately downregulated in human diabetes. *Nat Genet, 34*(3),
897 267-273. doi:10.1038/ng1180

898 Moynihan, K. D., Opel, C. F., Szeto, G. L., Tzeng, A., Zhu, E. F., Engreitz, J. M., . . . Irvine, D. J.
899 (2016). Eradication of large established tumors in mice by combination immunotherapy
900 that engages innate and adaptive immune responses. *Nat Med, 22*(12), 1402-1410.
901 doi:10.1038/nm.4200

902 Mueller, D. L. (2010). Mechanisms maintaining peripheral tolerance. *Nature Immunology, 11*(1),
903 21-27. doi:10.1038/ni.1817

904 Nelson, C. E., Mills, L. J., McCurtain, J. L., Thompson, E. A., Seelig, D. M., Bhela, S., . . .
905 Vezys, V. (2019). Reprogramming responsiveness to checkpoint blockade in
906 dysfunctional CD8 T cells. *Proc Natl Acad Sci U S A*. doi:10.1073/pnas.1810326116

907 Obar, J. J., Khanna, K. M., & Lefrançois, L. (2008). Endogenous naive CD8+ T cell precursor
908 frequency regulates primary and memory responses to infection. *Immunity, 28*(6), 859-
909 869. doi:10.1016/j.immuni.2008.04.010

910 Obar, J. J., Molloy, M. J., Jellison, E. R., Stoklasek, T. A., Zhang, W., Usherwood, E. J., &
911 Lefrançois, L. (2010). CD4+ T cell regulation of CD25 expression controls development
912 of short-lived effector CD8+ T cells in primary and secondary responses. *Proc Natl Acad*
913 *Sci U S A, 107*(1), 193-198. doi:10.1073/pnas.0909945107

914 Ozga, A. J., Moalli, F., Abe, J., Swoger, J., Sharpe, J., Zehn, D., . . . Stein, J. V. (2016). pMHC
915 affinity controls duration of CD8+ T cell-DC interactions and imprints timing of effector
916 differentiation versus expansion. *J Exp Med, 213*(12), 2811-2829.
917 doi:10.1084/jem.20160206

918 Palmer, E. (2003). Negative selection - Clearing out the bad apples from the T-cell repertoire.
919 *Nature Reviews Immunology, 3*(5), 383-391. doi:10.1038/nri1085

920 Parkhurst, M. R., Fitzgerald, E. B., Southwood, S., Sette, A., Rosenberg, S. A., & Kawakami, Y.
921 (1998). Identification of a shared HLA-A*0201 restricted T-cell epitope from the
922 melanoma antigen tyrosinase-related protein 2 (TRP2). *Cancer Research, 58*(21), 4895-
923 4901.

924 Pauken, K. E., Sammons, M. A., Odorizzi, P. M., Manne, S., Godec, J., Khan, O., . . . Wherry,
925 E. J. (2016). Epigenetic stability of exhausted T cells limits durability of reinvigoration by
926 PD-1 blockade. *Science, 354*(6316), 1160-1165. doi:10.1126/science.aaf2807

927 Philip, M., Fairchild, L., Sun, L., Horste , E. L., Camara , S., Shakiba , M., . . . Schietinger, A.
928 (2017). Chromatin states define tumour-specific T cell dysfunction and reprogramming.
929 *Nature, 545*, 452-456. doi:doi:10.1038/nature22367

930 Preston, G. C., Sinclair, L. V., Kaskar, A., Hukelmann, J. L., Navarro, M. N., Ferrero, I., . . .
931 Cantrell, D. A. (2015). Single cell tuning of Myc expression by antigen receptor signal
932 strength and interleukin-2 in T lymphocytes. *EMBO J, 34*(15), 2008-2024.
933 doi:10.15252/embj.201490252

934 Redmond, W. L., & Sherman, L. A. (2005). Peripheral tolerance of CD8 T lymphocytes.
935 *Immunity, 22*(3), 275-284. doi:10.1016/j.immuni.2005.01.010

936 Richards, D. M., Kyewski, B., & Feuerer, M. (2016). Re-examining the Nature and Function of
937 Self-Reactive T cells. *Trends in Immunology, 37*(2), 114-125.
938 doi:10.1016/j.it.2015.12.005

939 Richards, D. M., Ruggiero, E., Hofer, A. C., Sefrin, J. P., Schmidt, M., von Kalle, C., & Feuerer,
940 M. (2015). The Contained Self-Reactive Peripheral T Cell Repertoire: Size, Diversity,
941 and Cellular Composition. *Journal of Immunology, 195*(5), 2067-2079.
942 doi:10.4049/jimmunol.1500880

943 Rosenberg, S. A. (2014). IL-2: the first effective immunotherapy for human cancer. *J Immunol,*
944 *192*(12), 5451-5458. doi:10.4049/jimmunol.1490019

945 Sabatino, J. J., Huang, J., Zhu, C., & Evavold, B. D. (2011). High prevalence of low affinity
946 peptide-MHC II tetramer-negative effectors during polyclonal CD4+ T cell responses. *J*
947 *Exp Med, 208*(1), 81-90. doi:10.1084/jem.20101574

948 Saligrama, N., Zhao, F., Sikora, M. J., Serratelli, W. S., Fernandes, R. A., Louis, D. M., . . .
949 Davis, M. M. (2019). Opposing T cell responses in experimental autoimmune
950 encephalomyelitis. *Nature, 572*(7770), 481-487. doi:10.1038/s41586-019-1467-x

951 Schietinger, A., Delrow, J. J., Basom, R. S., Blattman, J. N., & Greenberg, P. D. (2012).
952 Rescued Tolerant CD8 T Cells Are Preprogrammed to Reestablish the Tolerant State.
953 *Science, 335*(6069), 723-727. doi:10.1126/science.1214277

954 Schietinger, A., & Greenberg, P. D. (2014). Tolerance and exhaustion: defining mechanisms of
955 T cell dysfunction. *Trends in Immunology, 35*(2), 51-60. doi:10.1016/j.it.2013.10.001

956 Shiow, L. R., Rosen, D. B., Brdicková, N., Xu, Y., An, J., Lanier, L. L., . . . Matloubian, M.
957 (2006). CD69 acts downstream of interferon-alpha/beta to inhibit S1P1 and lymphocyte
958 egress from lymphoid organs. *Nature, 440*(7083), 540-544. doi:10.1038/nature04606

959 Steitz, J., Brück, J., Lenz, J., Büchs, S., & Tüting, T. (2005). Peripheral CD8+ T cell tolerance
960 against melanocytic self-antigens in the skin is regulated in two steps by CD4+ T cells
961 and local inflammation: implications for the pathophysiology of vitiligo. *J Invest Dermatol,*
962 *124*(1), 144-150. doi:10.1111/j.0022-202X.2004.23538.x

963 Stuart, T., Butler, A., Hoffman, P., Hafemeister, C., Papalexi, E., Mauck, W. M., . . . Satija, R.
964 (2019). Comprehensive Integration of Single-Cell Data. *Cell, 177*(7), 1888-1902.e1821.
965 doi:10.1016/j.cell.2019.05.031

966 Su, L. F., Kidd, B. A., Han, A., Kotzin, J. J., & Davis, M. M. (2013). Virus-specific CD4(+)
967 memory-phenotype T cells are abundant in unexposed adults. *Immunity, 38*(2), 373-383.
968 doi:10.1016/j.immuni.2012.10.021

969 Subramanian, A., Tamayo, P., Mootha, V. K., Mukherjee, S., Ebert, B. L., Gillette, M. A., . . .
970 Mesirov, J. P. (2005). Gene set enrichment analysis: a knowledge-based approach for
971 interpreting genome-wide expression profiles. *Proc Natl Acad Sci U S A, 102*(43),
972 15545-15550. doi:10.1073/pnas.0506580102

973 Träger, U., Sierro, S., Djordjevic, G., Bouzo, B., Khandwala, S., Meloni, A., . . . Simon, A. K.
974 (2012). The immune response to melanoma is limited by thymic selection of self-
975 antigens. *PLoS One, 7*(4), e35005. doi:10.1371/journal.pone.0035005

976 Valenzuela, J., Schmidt, C., & Mescher, M. (2002). The roles of IL-12 in providing a third signal
977 for clonal expansion of naive CD8 T cells. *J Immunol, 169*(12), 6842-6849.

978 Waithman, J., Gebhardt, T., Davey, G. M., Heath, W. R., & Carbone, F. R. (2008). Cutting edge:
979 Enhanced IL-2 signaling can convert self-specific T cell response from tolerance to
980 autoimmunity. *J Immunol, 180*(9), 5789-5793. doi:10.4049/jimmunol.180.9.5789

981 Wang, R. F., Appella, E., Kawakami, Y., Kang, X., & Rosenberg, S. A. (1996). Identification of
982 TRP-2 as a human tumor antigen recognized by cytotoxic T lymphocytes. *J Exp Med,*
983 *184*(6), 2207-2216. doi:10.1084/jem.184.6.2207

Weninger, W., Crowley, M. A., Manjunath, N., & von Andrian, U. H. (2001). Migratory properties of naive, effector, and memory CD8(+) T cells. *J Exp Med, 194*(7), 953-966.

Wickham, H. (2016). *ggplot2: Elegant Graphics for Data Analysis*. New York: Springer-Verlag.

Yu, W., Jiang, N., Ebert, P. J. R., Kidd, B. A., Muller, S., Lund, P. J., . . . Davis, M. M. (2015). Clonal Deletion Prunes but Does Not Eliminate Self-Specific alpha beta CD8(+) T Lymphocytes. *Immunity, 42*(5), 929-941. doi:10.1016/j.immuni.2015.05.001

Zehn, D., & Bevan, M. J. (2006). T cells with low avidity for a tissue-restricted antigen routinely evade central and peripheral tolerance and cause autoimmunity. *Immunity, 25*(2), 261-270. doi:10.1016/j.immuni.2006.06.009

Zehn, D., Lee, S. Y., & Bevan, M. J. (2009). Complete but curtailed T-cell response to very low-affinity antigen. *Nature, 458*(7235), 211-214. doi:10.1038/nature07657

Zhang, S., Bernard, D., Khan, W. I., Kaplan, M. H., Bramson, J. L., & Wan, Y. (2009). CD4+ T-cell-mediated anti-tumor immunity can be uncoupled from autoimmunity via the STAT4/STAT6 signaling axis. *Eur J Immunol, 39*(5), 1252-1259. doi:10.1002/eji.200839152

Zheng, G. X., Terry, J. M., Belgrader, P., Ryvkin, P., Bent, Z. W., Wilson, R., . . . Bielas, J. H. (2017). Massively parallel digital transcriptional profiling of single cells. *Nat Commun, 8*, 14049. doi:10.1038/ncomms14049

Non-standard abbreviations

Dct$^{-/-}$, dopamine tautomerase deficient
DNFB, dinitrofluorobenzene
LmTrp2, *Listeria monocytogenes* strain expressing Trp2
MFI, median fluorescence intensity
Treg, regulatory T cell
Trp2, tyrosinase-related protein 2
UMAP, uniform manifold approximation and projection

Supplemental figures

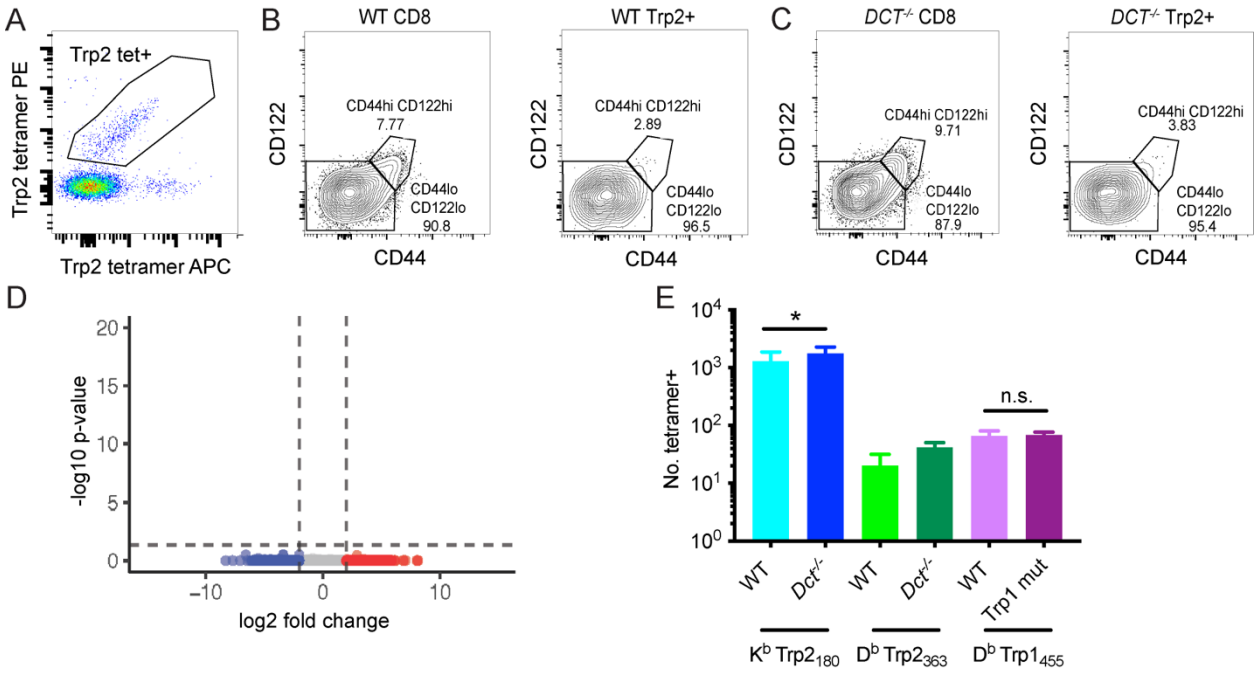

Supplemental figure 1. Additional analysis of the Trp2/K^b-specific population and cells specific for other melanocyte epitopes in pre-immune mice.
(A) Tetramer staining of pre-immune lymphocytes (enriched fraction, gated on live, dump-negative CD8+ T cells). Dual tetramer staining was used to facilitate more accurate gating on antigen-specific cells. (B, C) CD44 and CD122 staining of pre-immune Trp2/K^b-specific cells from a WT mouse (B) and a *Dct*$^{-/-}$ mouse (C). (D) Bulk RNA sequencing of Trp2/K^b-specific CD8+ T cells from pre-immune WT and *Dct*$^{-/-}$ mice was performed; differentially expressed genes were not identified between WT and *Dct*$^{-/-}$ samples as shown by the volcano plot. (E) Quantification of CD8+ T cells specific for a D^b-restricted Trp2 epitope and an epitope from tyrosinase-related protein 1 (Trp1) in pre-immune mice reveals a similar or slightly lesser number of cells in mice expressing antigen (WT mice) relative to those that do not. Samples used for tetramer enrichment of Trp1/D^b-specific cells were obtained from shipped samples; accordingly, these data likely underestimate the precursor frequency. PC, principal component. * $p < .05$ by one-way ANOVA with Sidak's multiple comparisons test.

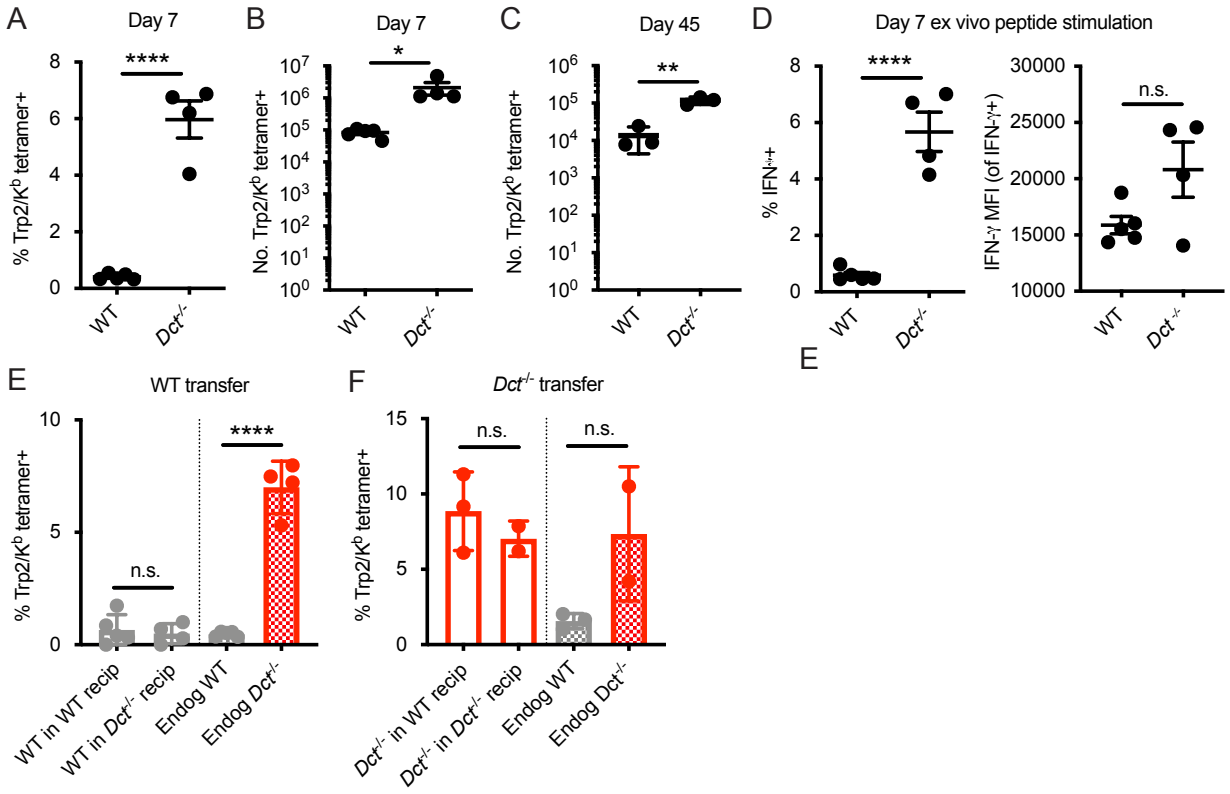

Supplemental figure 2. Response to infection with LmTrp2 in primary and transfer settings
Mice were infected with a recombinant *Listeria monocytogenes* strain expressing Trp2 (LmTrp2; A–D). The percent (A) or number (B, C) of splenic Trp2/K^b-specific cells was assessed at the indicated day. (D) Day 7 splenocytes were stimulated for 4–6 hours with Trp2 peptide and intracellular staining was performed to assess cytokine production. (E, F) CD8+ T cells from pre-immune WT or *Dct*$^{-/-}$ donors were negatively enriched and bulk CD8+ T cells were transferred into congenically distinct WT or *Dct*$^{-/-}$ recipients. One day later, mice were infected with LmTrp2. Donor and endogenous cells were collected from the blood of recipient mice on day 7 following infection and assessed for Trp2/K^b tetramer binding. Data in A, B, and D are representative of 3 similar experiments; data in C, E, and F represent individual experiments with 2–5 mice per group. Squares indicate male animals. * $p < 0.05$, ** $p < 0.01$, *** $p < 0.001$, **** $p < 0.0001$ by unpaired t test (A–D) or one-way ANOVA with Sidak's multiple comparisons test (E, F). Endog, endogenous; recip, recipients.

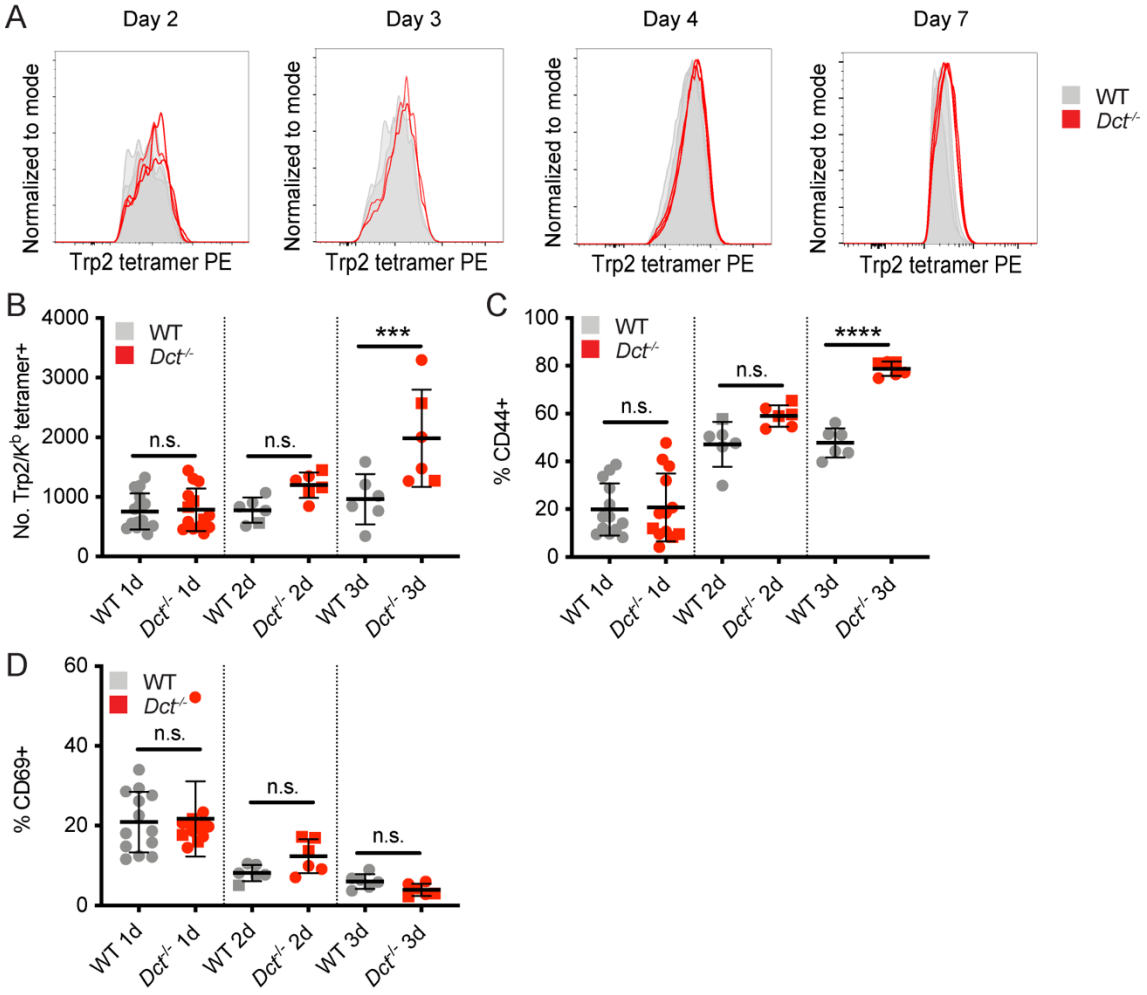

Supplemental figure 3. Tetramer staining kinetics and response to peptide immunization. WT and *Dct*$^{-/-}$ mice received intravenous injections of 200 ug Trp2 peptide as part of TriVax (A) or alone (B–D). (A) Histograms of tetramer staining for Trp2/K^{b}-binding cells. (B–D) Tetramer enrichment was used to enumerate Trp2/K^{b}-specific cells and assess their phenotype at the indicated time points following peptide injection; males are indicated by square symbols. Data from representative experiments at each time point are shown in (A). Data in B–D are compiled from multiple experiments. *** $p < 0.001$, **** $p < 0.0001$ by one-way ANOVA with Sidak's multiple comparisons test.

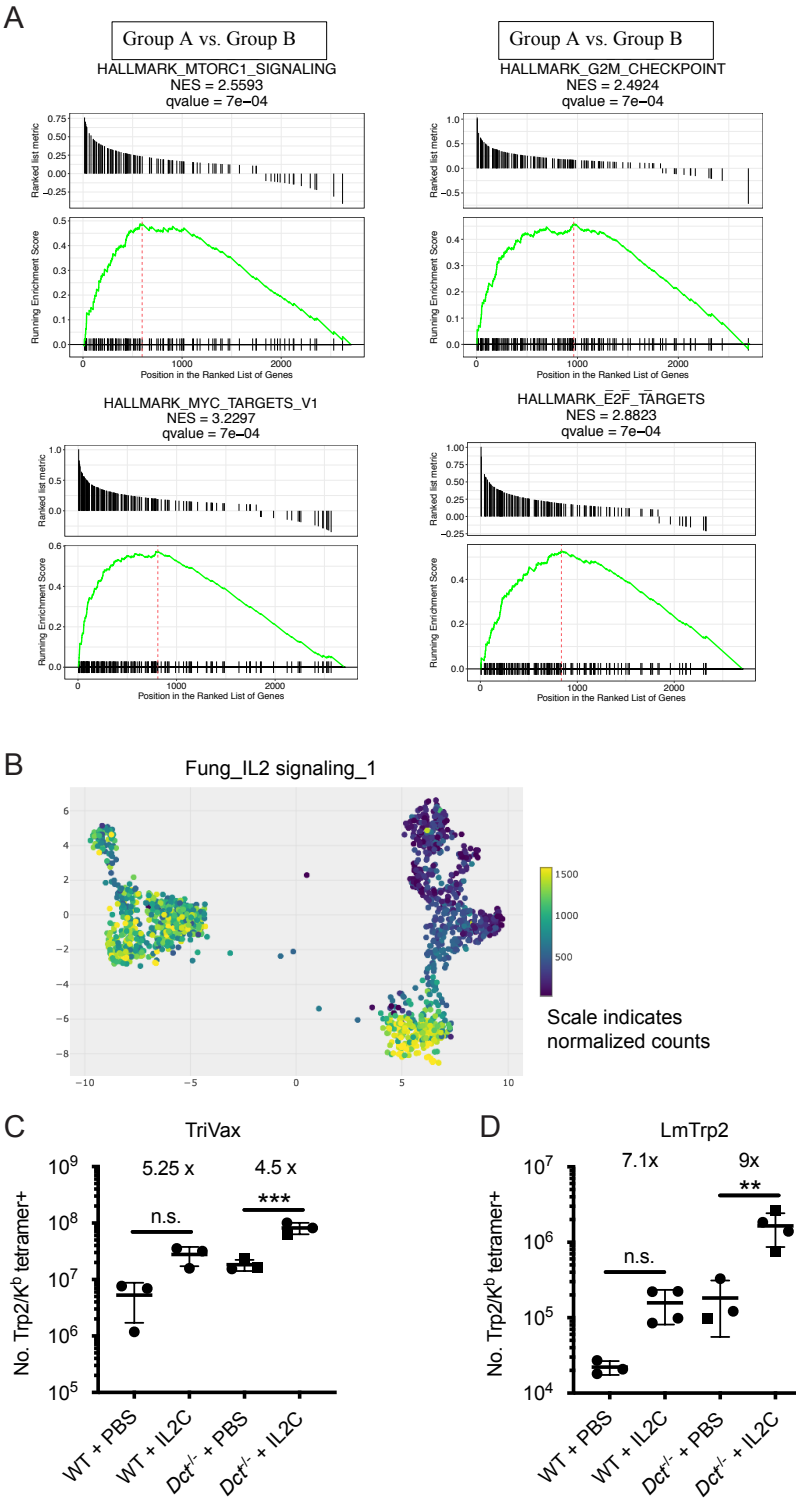

Supplemental figure 4. GSEA of single-cell data and response of WT and *Dct*$^{-/-}$ Trp2/K^{b}-specific cells to IL-2C
(A) Gene set enrichment analysis (GSEA) plots show enrichment of the following gene sets in Group A: Myc targets, MTORC1 signaling, G2M checkpoint, E2F targets. (B) Enrichment between clusters and a dataset of genes involved in IL-2 signaling is indicated by color. (C, D) WT and *Dct*$^{-/-}$ mice were immunized with TriVax (C) or infected with LmTrp2 (D) and treated with PBS or IL-2C on day five. Trp2/K^{b} tetramer positive splenocytes were enumerated on day seven after priming/infection. Squares indicate male animals. * $p < 0.05$, **** $p < 0.0001$ by one-way ANOVA with Tukey's multiple comparisons test. IL-2C, IL-2 complex.

A

Vitiligo scoring metric

Score	Description
0	No vitiligo
1	Possible vitiligo
2	Definite but limited vitiligo: some hair or a small tuft
3	Small patch of vitiligo
4	Large patch of vitiligo (> 1 cm^2) or multiple small patches
5	Extensive vitiligo (multiple large patches, patch + many hairs, etc.)

D

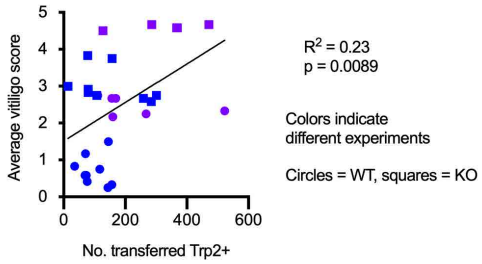

B

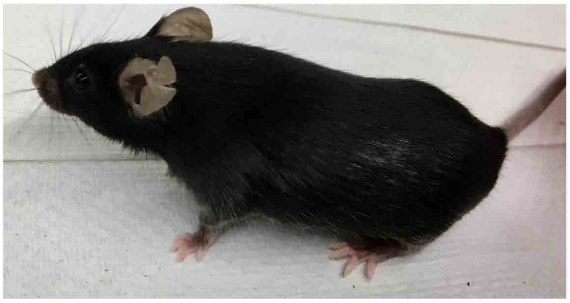

Example of a grade 2 mouse (received WT cells)

C

Example of a grade 5 mouse (received *Dct*$^{-/-}$ cells)

Supplemental figure 5. Vitiligo scoring metric and correlation between the average vitiligo score and the number of transferred Trp2/K^b-specific cells

(A) Vitiligo scoring metric used to quantify the degree of vitiligo. (B) Example of a grade 2 mouse; (C) example of a grade 5 mouse. (D) Average vitiligo score per mouse (days 0–93) relative to the number of transferred Trp2/K^b tetramer positive cells on day six after transfer and TriVax boost. Two compiled experiments are shown. Simple linear regression was used to fit a line and assign R^2 and p-values.